NUREG/CR-4379
Vol. 3

Long-Term Performance of Materials Used for High-Level Waste Packaging

Third Quarterly Report, Year Four
October - December 1985

Compiled by D. Stahl, N. E. Miller

Battelle's Columbus Division

Prepared for
U.S. Nuclear Regulatory
Commission

NUREG/CR-4379
Vol. 3

Long-Term Performance of Materials Used for High-Level Waste Packaging

Third Quarterly Report, Year Four
October - December 1985

Manuscript Completed: February 1986
Date Published: March 1986

Compiled by
D. Stahl, N. E. Miller

Battelle's Columbus Division
505 King Avenue
Columbus, OH 43201-2693

Prepared for
Division of Radiation Programs and Earth Sciences
Office of Nuclear Regulatory Research
U.S. Nuclear Regulatory Commission
Washington, D.C. 20555
NRC FIN B6764
Under Contract No. NRC-04-82-015

PREVIOUS REPORTS IN SERIES

NUREG/CR-3405, Volume 1: "Long-Term Performance of Materials Used for High-Level Waste Packaging: Annual Report, March 1982-April 1983."

NUREG/CR-3427, Volume 1: "Long-Term Performance of Materials Used for High-Level Waste Packaging: Quarterly Report, April-June 1983."

NUREG/CR-3427, Volume 2: "Long-Term Performance of Materials Used for High-Level Waste Packaging: Quarterly Report, July-September 1983."

NUREG/CR-3427, Volume 3: "Long-Term Performance of Materials Used for High-Level Waste Packaging: Quarterly Report, October-December 1983."

NUREG/CR-3427, Volume 4: "Long-Term Performance of Materials Used for High-Level Waste Packaging: Annual Report, April 1983-April 1984."

NUREG/CR-3900, Volume 1: "Long-Term Performance of Materials Used for High-Level Waste Packaging: Quarterly Report, April-June 1984."

NUREG/CR-3900, Volume 2: "Long-Term Performance of Materials Used for High-Level Waste Packaging: Quarterly Report, July-September 1984."

NUREG/CR-3900, Volume 3: "Long-Term Performance of Materials Used for High-Level Waste Packaging: Quarterly Report, October-December 1984."

NUREG/CR-3900, Volume 4: "Long-Term Performance of Materials Used for High-Level Waste Packaging: Annual Report, April 1984-April 1985.

NUREG/CR-4379, Volume 1: "Long-Term Performance of Materials Used for High-Level Waste Packaging: Quarterly Report, April-June 1985.

NUREG/CR-4379, Volume 2: "Long-Term Performance of Materials Used for High-Level Waste Packaging: Quarterly Report, July-September 1985.

ABSTRACT

As part of the information needed by the Nuclear Regulatory Commission to assess the Department of Energy's application to construct geologic repositories for high-level radioactive waste, Battelle's Columbus Division is investigating the long-term performance of materials used for high-level waste packages. Waste-form studies are being directed toward investigating spent-fuel leaching/dissolution behavior. Experiments have been started to generate data on UO_2 and spent-fuel leach rates in simulated anoxic groundwaters. Initial data indicate that uranium concentrations in the groundwaters and distilled-water leachants are very low. The influence of groundwater species on the susceptibility of cast steel to pitting corrosion and stress-corrosion cracking is being studied by potentiodynamic polarization techniques. Potential cracking agents are being investigated by slow strain rate experiments. The pitting-corrosion model was further developed, taking into account cation dissolution at the pit base and chemically active pit walls. Groundwater-radiolysis modeling has continued, with the description being extended to include bicarbonate anions in groundwater. Simulations show that modifications to the reactions accounting for bicarbonate should improve predicted pH values. Spent-fuel specimens are being used in integral tests with flowing simulated groundwater to study the role of cladding in radionuclide release and to identify possible combined-effects processes.

This report documents investigations performed during the period October 1985 through December 1985.

TABLE OF CONTENTS

TABLE OF CONTENTS
(Continued)

LIST OF FIGURES

LIST OF FIGURES
(Continued)

LIST OF TABLES

CONTRIBUTORS

J. A. Beavers
R. Kohli
A. J. Markworth
J. K. McCoy
J. L. Means
S. L. Nicolosi
R. Rungta
S. W. Rust
E. D. Spinosa
N. G. Thompson

1. INTRODUCTION: PROJECT OBJECTIVES AND APPROACH

The Waste Policy Act of 1982 delegates to the Department of Energy (DOE) the authority for siting, construction, and operation of deep-mined geologic repositories for the disposal of high-level waste and spent fuel. The Nuclear Regulatory Commission (NRC) has the responsibility to regulate the activities of DOE to assure that the health and safety of the repository workers and of the public are adequately protected. Prior to construction, the DOE will submit a license application to the NRC describing in detail the proposed repository. The DOE has been directed to take a multiple barrier approach to the isolation of radioactive wastes with the waste package, the underground facility, and the natural geohydrologic features of the site being the major barriers. Since NRC's compliance assessment requires the technical capability to understand relevant phenomena and processes relating to the long-term performance of the multiple barriers, the NRC's Office of Nuclear Regulatory Research (RES) has established this waste-package performance program at Battelle's Columbus Division to provide that part of the input to the assessment. As an important aid to this understanding, Battelle is evaluating total system performance by integrating a variety of processes that effect the long-term performance of waste-package materials. This systems approach also serves to identify and evaluate research needs.

After the repository is closed, the dominant mechanism to cause the release of radionuclides from the repository is assumed to be groundwater transport. The generally accepted approach to minimizing the release is to provide a number of different barriers to the dissolution and transport of radionuclides by the groundwater. For a deep-mined repository, the geohydrologic features of the earth itself are expected to be a major barrier to the release of radionuclides. The repository site will be selected so that radionuclides will be isolated for very long times. In addition, engineered features of the repository will act as a barrier to the release of radionuclides. The repository will be constructed so as to minimize disturbing the adjacent rock and to accommodate the thermomechanical effects of the emplaced wastes with a minimum of degradation to its geohydrologic properties. Upon closure, the underground openings and shafts to the surface will be backfilled and sealed to minimize groundwater flow paths.

The waste package--which is the center of this study--will be constructed to provide essentially complete containment of the radionuclides through the period of time in which the repository is heated significantly by decaying fission products. After the container is eventually breached by some process, the waste form must remain sufficiently resistant to groundwater attack to provide high retention of the radionuclides and, together with the repository, to control the release of radionuclides for thousands of years. The objective of our research is to provide an improved understanding of the long-term performance of the materials used for the high-level waste package. More specifically, we are identifying those processes that tend to degrade the performance of the waste-package materials, performing experiments to produce data

where data are otherwise lacking on material performance, and analytically modeling the processes to utilize the data more effectively. In addition, we are identifying areas of work that should be performed by DOE to provide missing data which are beyond the resources of the NRC.

1.1 Individual Program Tasks

The program is being conducted in three parallel efforts: waste-form studies, overpack corrosion studies, and integrated system performance studies. A more detailed summary of achievements can be found in the second annual report for this program (NUREG/CR-2127, Volume 4, July 1985, Section 1).

1.1.1 Waste Forms

The waste-form studies are aimed at first describing and modeling those mechanisms that will alter or "age" the waste form during the containment period, and second, identifying and describing those processes that will influence waste-form dissolution after it is exposed to groundwater. The waste-form studies have previously centered on borosilicate glasses, and experiments have been performed to investigate the long-term dissolution/reprecipitation behavior of simulated waste glass and the effects of crystallinity influences. However, emphasis is now being directed toward evaluating spent fuel as a waste form. In particular, the leach/dissolution behavior of spent fuel and the effects of cladding in radionuclide release are being studied.

Three spent-fuel leaching experiments have been planned that will provide a definite comparison of the leach behaviors of unirradiated and irradiated fuels in repository-relevant environments. Spent-fuel and UO_2 specimens will be exposed to different types of low-flow, anoxic simulated groundwater and radiation field conditions. These experiments, one of which is in progress, will be used to investigate spent-fuel solubility and possible selective leaching of radionuclides.

1.1.2 Overpack Corrosion

The overpack corrosion studies focus on processes that can degrade the metallic waste-package overpack. The objective is to collect data on the parameters that influence the degradation processes, to identify the controlling parameters, and ultimately to model the degradation processes that determine the long-term performance of the overpack. The material under study is cast low-carbon steel; this material is currently favored by DOE for use in a basalt repository.

The dominant degradation processes that affect the outside of the overpack are general corrosion, stress-corrosion cracking, pitting, crevice corrosion, hydrogen attack, and mechanical stress. These processes may occur individually or in combination. The parameters that affect these processes include chemical composition and physical state of the steel, groundwater composition and flow rate, temperature, radiation intensity, availability of air, lithostatic forces, redox state, alkalinity or

acidity, and availability of hydrogen. These can produce general corrosion, in which the rate of general corrosion will determine the necessary wall thickness, or localized corrosion (such as pitting or crevice corrosion), in which the rate of the localized attack and the container life must be used to establish the wall thickness.

If the steel is susceptible to cracking in the expected environment, the rate of cracking is so rapid relative to required container life that the corrosion-allowance approach cannot be used to achieve acceptable performance. What is important is the susceptibility of the metal to crack initiation and propagation. Cracking may result from stress-corrosion cracking or from reduction in fracture toughness from hydrogen attack. Both of these processes are under investigation.

In addition, a comprehensive mathematical model is under development for use in understanding the corrosion processes associated with the waste-container materials in a repository environment. The model computes the fluxes of corrosive species to the overpack surface, taking into account the fact that certain corrosive species may be generated by radiolysis, and also accounts for diffusion and convective flow to transport the species. The modeling effort is also being applied to pitting attack and considers three different aspects of the overall pitting process: pit-initiation kinetics, pit-growth kinetics, and the evolution of the pit-depth distribution. These analytical efforts are well integrated with the experimental efforts and are directed to providing an understanding of the long-term performance of the overpack materials, with emphasis on those processes that can lead to poor performance.

1.1.3 Integrated System Performance

The waste-package system performance studies are an interface between the waste-form studies and the container-material studies to provide an improved understanding of the performance of the total waste-package system. The current emphasis is on the processes involved in waste-package system degradation. One aspect of the total system under study is the production of radiolysis products in the groundwater by gamma radiation from the waste. This is of major importance in modeling the corrosion of the overpack and in planning experiments to determine the effects of radiolysis. Our radiolysis model is based on existing codes and sets of chemical reactions combined to provide the best description of experimental data found in the literature. The output of the radiolysis model calculations provides input to the water-chemistry model, which is a fundamental part of the glass-dissolution model and the general-corrosion model.

The water-chemistry model which we initially developed for our use with our glass-dissolution and corrosion models has intentionally been kept simple. Simplifying assumptions were made and only a limited set of chemical species was used. This model calculates the concentration and activity of each of the species in the water.

Integral tests have been designed and are being performed using spent-fuel specimens. Simulated groundwater is passed over these specimens and then analyzed to investigate the effects on radionuclide release of potential repository conditions. These tests will explore the role of the cladding in radionuclide release and will aid in assessing combined-effects processes that may affect waste-package integrity.

1.2 Overall Program Objectives

In all the program tasks, the ultimate objective is to develop a base of information to assist the NRC in evaluating the performance of the waste package proposed in DOE's license application. A near-term objective is to provide information to allow the NRC to prepare position papers on the information required of DOE for evaluation of their waste package. Of significance here is identifying sensitive parameters affecting the performance of materials and identifying data requirements.

To achieve the above objectives, the waste-form task is providing information to give a better understanding of the release of radionuclides from the waste form, beginning at the time it is first contacted by groundwater, through the 10,000-year period defined in the EPA Standard. This includes an understanding of the probable physiochemical condition of the waste form when it is contacted by groundwater, as well as the parameters of waste-form composition and environmental conditions which will cause changes from its state at the time of disposal. In addition, we are producing experimental data on the parameters that affect dissolution of the waste form, including composition of the groundwater and environmental conditions. The waste-form dissolution process is also being mathematically modeled to allow analysis of the performance of the waste form under specific input conditions.

The information on the performance of the overpack materials relates to the required containment period of 300 to 1000 years. Overpack performance is expected to be most affected by corrosion and hydrogen-attack processes. We are attempting to provide information on the parameters of overpack-material composition, groundwater composition, and environmental conditions that are most significant in these processes. Our preliminary study of the titanium alloy in brine did not reveal any conditions that would cause general corrosion, pitting, crevice corrosion, or stress-corrosion cracking to affect the good performance of the material as claimed in the literature. However, vapor-phase attack was identified; this could degrade the material and should be more thoroughly investigated if the DOE selects this material for use.

Our studies of cast low-carbon steel in a basalt environment are currently focused on the susceptibility of the metal to stress-corrosion cracking under repository conditions, because steel is known to fail by this process in some environments. We are studying the chemical species and environmental conditions that cause cracking to determine whether this mode of failure is expected under credible repository conditions. Our experimental studies on general and localized corrosion, together with our comprehensive general-corrosion model, will assist in

evaluating the corrosion-allowance approach for the use of steel as a long-life container.

Although the development of an integrated waste-package system model is no longer included in the scope of this project, modeling efforts in the integrated system-performance task are contributing significant information to studies of general corrosion and glass and spent-fuel dissolution. These studies require knowledge of the amount and kind of chemical species that may be produced by radiolysis of the groundwater near the waste package as a result of gamma radiation from the enclosed waste. To obtain this information, energy deposition and radiolysis codes are used. To determine how these radiolysis products may affect the performance of the overpack and waste form, their chemical activities are calculated by the water-chemistry model, using as input data from experiments and from the groundwater-radiolysis model. The output from the water-chemistry model is the concentration and activity of each chemical species in the groundwater near the waste package. This information is used not only as input to the general-corrosion and glass-dissolution models but also as a point of reference in directing the experimental efforts in corrosion and dissolution. Some effects of radiolysis may be observed in the integral experiments that are being conducted. The integral experiments will provide insight into the role of cladding in the release of radionuclides from spent fuel and will help to identify certain combined-effects processes, possibly synergistic in nature, that may affect the performance of the overpack and waste form.

2. WASTE FORMS

Waste-form experimentation is being directed away from an emphasis on glass leaching to the leaching/dissolution behavior of unirradiated and spent fuel. During this quarter, a 32-day experiment evaluating the leaching behavior of devitrified MCC 76-68 simulated waste glass was conducted. The analysis of leachates (to be conducted next quarter) from this experiment will conclude our efforts on glass-leaching experimentation. Important results obtained this quarter from the glass-dissolution and crystallinity experiments are summarized in Sections 2.1.1 and 2.1.2, respectively.

Three different spent-fuel leaching experiments have been planned, the first of which was started last quarter. These experiments will be comprised of the following test specimens and conditions:

- Unirradiated UO_2--no external radiation field
- Unirradiated UO_2--external radiation field
- Irradiated fuel.

The experiments will be carried out with the specimens placed in contact with flowing simulated tuff, basalt, and brine groundwater and distilled water. Each of the tests will be conducted for a minimum of nine months, or until steady-state leach rates are observed. Progress on the first of these tests this quarter is described in Section 2.2.1.

Waste-form dissolution modeling has continued, and results of the glass dissolution experiments have been compared to the model to validate an analytic description of the dissolution/reprecipitation kinetics.

2.1 Glass Experiments

2.1.1 Glass-Dissolution Model Verification

The results of an experiment to verify a numerical model for the long-term dissolution and reprecipitation behavior of MCC 76-68 simulated waste glass in water at 90 C have been reported at length in the previous two quarterly reports. In summary, we have observed that at 90 C, silica dissolving from MCC 76-68 reprecipitates as a crystalline zinc silicate phase, probably willemite, in the glass surface alteration layer. The zinc silicate precipitate controls the solubility (and hence, the dissolution rate) of silica in the leachate at a value intermediate between the experimental solubility of amorphous silica and the calculated solubility of $ZnSiO_3$, which approximates the composition of the observed reprecipitate. After an initial equilibration period (represented by time equivalents of 0 to around 2,500 days/meter in Figure 2.1), the solubility of silica in the leachate levels off, reflecting steady-state kinetics between the dissolution and reprecipitation reactions. The quantity of zinc silicate crystals in the alteration layer increases with time, as observed in scanning electron microphotographs. The data in Figure 2.1 have been fitted by a first-order

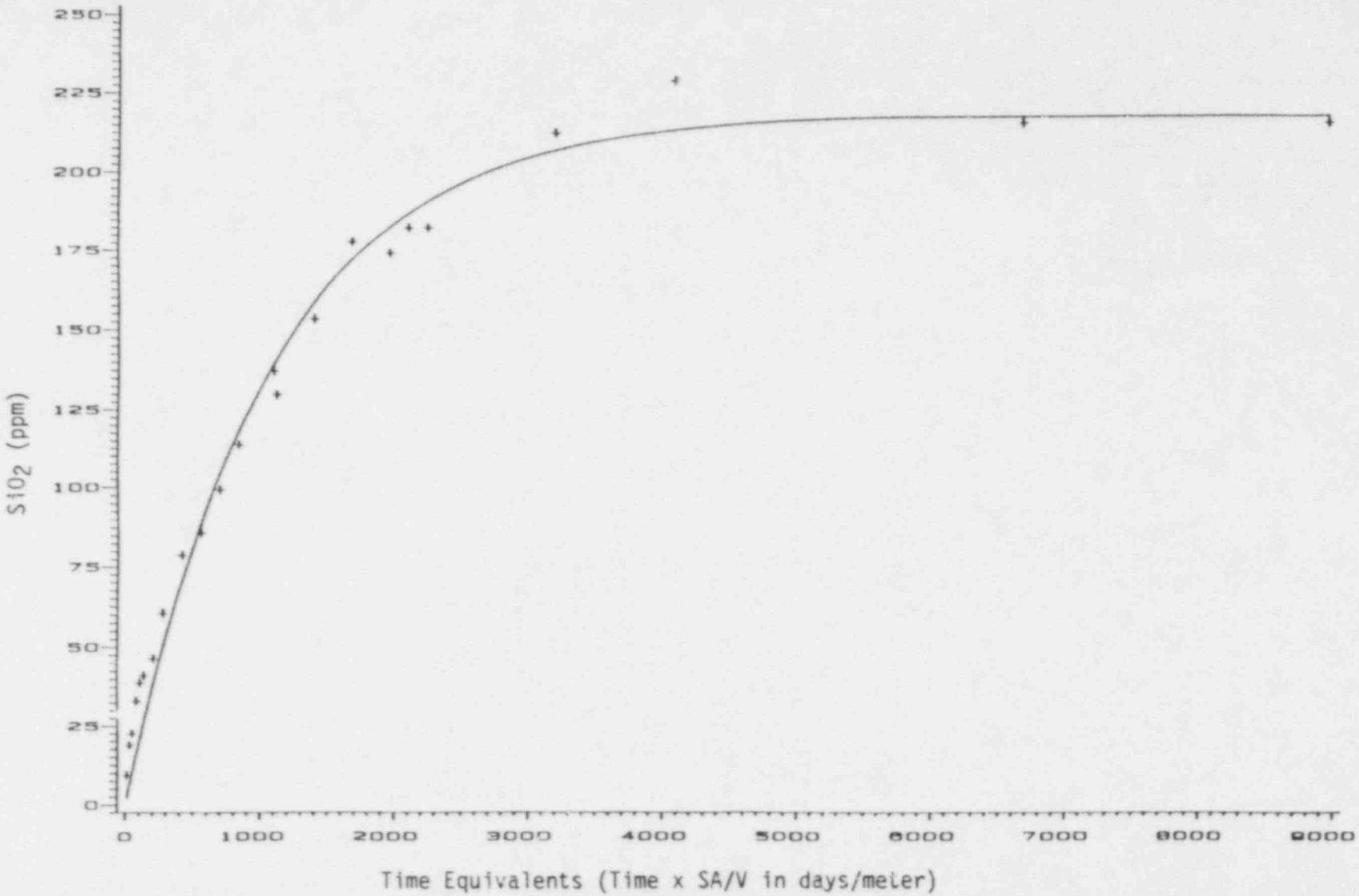

Figure 2.1. Results of the glass dissolution rate model verification experiments.

regression analysis, yielding rate constants of 5.382×10^{-4} for the dissolution reaction and 3.871×10^{-4} for the reprecipitation reaction.

The experimental aspects of this study have now been completed. Efforts in the near-term will be directed at preparing a manuscript for publication in a peer-reviewed journal.

2.1.2 Crystallinity Influences

The glass crystallinity experiment was completed at the end of this quarter. In brief, two sets of samples doped with RuO_2 as a heterogeneous nucleating agent were prepared for leach testing at 90 C. Three digestion bombs with high surface-area-to-volume ratios were prepared for each crystallinity condition, as were two reference bombs containing untreated MCC 76-68 glass. These samples were exposed to reagent-grade water at 90 C for 32 days, a time increment equivalent to one of the data points in the model-verification experiment. Exposure at these conditions was completed late in the reporting period.

The leachate for each bomb has been submitted for analysis of dissolved SiO_2. Once these analyses are complete, ICAP spectroscopic analyses will be used to determine the concentrations of rare earth oxides and selected transition metals in the leachates. Scanning electron microscopy (SEM) will be used as needed to investigate changes to the surface of the samples. The details of these analyses will be provided in the annual report for this project year next quarter.

2.2 Spent-Fuel Experiments

2.2.1 Experimental Leach Rate Experiments

The objective of the spent-fuel and UO_2 leach tests to be conducted under this program is to generate high-quality data on spent-fuel and UO_2 leach rates under expected repository (i.e., anoxic) conditions. As described previously, three different flow-through tests are being or will be conducted. The first of these, an evaluation of unirradiated UO_2 leach behavior in the absence of an external radiation field, was started November 16, 1985. The second and third tests are planned to begin in early February and early April, 1986, respectively.

All three tests will be conducted in nearly identical aqueous geochemical environments, except for the external radiation field. This will allow us to isolate and characterize the magnitude of the effect of radiolysis on UO_2 and spent-fuel leach rates. The most critical variables are shown in the second and third columns of Table 2.1. The leachates include a simulated brine[2.1] (WIPP Brine A), tuff[2.2] (Yucca Mountain J-13 well water), and basalt[2.3] groundwater as well as distilled water. The surface-area-to-volume (SA/V) ratio is also varied between 5 and 50 $meter^{-1}$ to evaluate the effect of this variable on UO_2 and spent-fuel leaching. The latter consideration is intended to facilitate evaluating solubility control on leach rates. Anoxic

Table 2.1. Results of UO_2 leach tests through day 50 of the experiments conducted in the absence of an external radiation field.

Reaction Vessel Number	Synthetic Leachate Composition	SA/V (meter^{-1})	Uranium Concentration (ppm) Day 20	Day 50
1	Brine	5	0.08	0.12
2	Brine	5	0.07	0.12
3	Brine	5	0.06	0.09
4	Brine	50	0.11	0.10
5	Brine	50	0.09	0.08
6	Tuff	5	< 0.01	0.01
7	Tuff	5	< 0.01	0.02
8	Tuff	5	< 0.01	< 0.01
9	Tuff	50	0.03	0.01
10	Tuff	50	0.01	< 0.01
11	Basalt	5	< 0.01	< 0.01
12	Basalt	5	< 0.01	0.01
13	Basalt	5	< 0.01	< 0.01
14	Basalt	50	0.04	0.03
15	Basalt	50	< 0.01	< 0.01
16	Distilled Water	5	< 0.01	< 0.01

conditions are being established and maintained using the method of Jantzen[2.4], who produced low redox potentials (i.e., -0.15 to -0.45 volts) in simulated groundwater by exposing it to high SA/V-ratio ductile iron. The carbon steel reaction vessel provides additional redox buffering capacity. Leachate redox potential will be established by a specially designed in situ Eh measurement device, which will allow the Eh of the leachate exiting the reaction vessel to be measured without contamination by atmospheric gases. This cell is currently being prepared and will be available for use in this program sometime next quarter.

All of the leach tests are flow-through in design, using pulsed flow. At least initially, leachate samples are being collected at a frequency of 20 to 30 days. At the time of sampling, the leachate that is being withdrawn from the experimental vessel is replenished with an identical volume of leachate, which has been equilibrated with ductile iron for at least 24 hours to consume oxygen and lower the redox potential. At each sampling, the volume of leachate collected is small in comparison with the total volume of leachate in the reaction vessel and is adjusted to yield an equivalent contact time of 1 year.

The results of the first experiment through day 50 are shown in Table 2.1. Total uranium concentrations in all of the 16 reaction vessels are very low, and the only statistically significant effect is that uranium concentrations in brine are several times higher than those in tuff and basalt groundwater and distilled water, which are barely detectable or not detectable at all by the fluorometric analysis procedure. We plan to continue to collect data on this experiment for at least another 315 days to determine any changes in UO_2 concentrations with time.

The second unirradiated UO_2 leaching experiment, which will be identical to the experiment described above except having an external radiation field of approximately 10^4 rads per hour, will be started in the next several weeks. The spent-fuel test is currently scheduled to begin early in Year 5 of this program. All three tests will be conducted for at least one year. This experimental plan, taken as a whole, is intended to be the definitive study for comparing the leach behaviors of unirradiated and irradiated fuel in repository-relevant chemical environments. This one-and-a-half year study should also show whether spent fuel is as insoluble as unirradiated UO_2 under anoxic conditions and if there is selective leaching of some radionuclides from spent fuel.

2.2.2 Quality Assurance Procedures

Two Quality Assurance Procedures were developed this quarter in conjunction with the Waste Forms Task. They are:

- Laboratory Procedure for the Preparation of Simulated WIPP Brine A, WF-PP-32, Revision 1, November 18, 1985

- Laboratory Procedure for the Fluorometric Analysis of Uranium in Ground Water and Brine, WF-PP-17, Revision 0, November 26, 1985.

2.2.3 Radionuclide Distribution in Spent Fuel

A task was started to summarize the available information on the distribution of selected radionuclides (Am, Cs, Np, Th, Pu, I, Sn, Sr, Tc, C) in spent fuel. These elements were selected on the basis of their long half-lifes and activity in spent fuel. The emphasis is on microscopic distribution (for example, within grains and grain boundaries) rather than macroscopic distribution of these radionuclides. This information will be very useful in analyzing the data generated in the spent-fuel leach rate studies and in the integral experiments.

During this quarter, initial discussions were held with personnel at the Karlsruhe Nuclear Research Center in West Germany and at Argonne National Laboratory on the feasibility of using analytical techniques such as electron microprobe analysis and Auger electron spectroscopy to characterize the distribution of the above radionuclides. In addition, the discussions also focused on the use of available theoretical models such as the Booth Diffusion Model[2.5, 2.6] or the FASTGRASS Model[2.7] to calculate the microscopic radionuclide inventory in spent fuels. Since these models assume radionuclide migration in vapor form, detailed knowledge of the chemical state of the radionuclides of interest is essential.

The assessment of available information will be completed next quarter. Gaps in the existing data base will be identified and areas of further experimental and/or theoretical work needed will be explored.

2.3 Waste-Form Dissolution Modeling

2.3.1 Extension of Glass Dissolution/Reprecipitation Model--Inclusion of Second-Order Reprecipitation Kinetics

For the glass dissolution/reprecipitation model developed earlier under this program[2.8, 2.9], both the glass-dissolution reaction and the precipitate-growth reaction were assumed to follow first-order kinetics, that is, to vary linearly with the supersaturation. Thus, the rate of glass dissolution was assumed to be proportional to $C_0 - C$ and the rate of precipitate growth to be proportional to $C_0' - C$, where C_0 and C_0' are the saturation concentrations in the groundwater of the species (silicon) controlling the kinetics, measured with respect to the glass and the precipitate, respectively, with C being the instantaneous concentration of dissolved silicon in the groundwater. The resultant model yielded a relatively good "fit" to the experimental data obtained under this program in the glass-dissolution experiment, as is shown in Figure 2.1.

It has been pointed out, however, (e.g., Hohmann and Kahlweit[2.10], Reich and Kahlweit[2.11]) that crystal growth from solution is, in general, determined by second-order kinetics, in which case the precipitate growth under present consideration would proceed at a rate proportional to $(C_o' - C)^2$. In this light, the dissolution/reprecipitation model developed earlier[2.8] was generalized to account for precipitate growth occurring by second-order kinetics, assuming still that the glass dissolution takes place via first-order kinetics.

For this case, Equation 2.21 of Reference 2.8 must be modified as follows:

$$\frac{dC}{dt} = \frac{KS}{V}(C_o - C) - K'(C_o' - C)^2 \qquad (2\text{-}1)$$

where t represents time, K is the rate-constant for glass dissolution, S the surface area of the glass, V the volume of solution, and K' an effective rate-constant for precipitate growth. Equation 2-1 is valid within the regime $C_o' \leq C \leq \bar{C}$. The constant K' may, in general, be dependent upon time, but only the simple case for which it is assumed to be time-dependent is considered here. This particular case was considered in detail, for first-order reprecipitation kinetics, in Reference 2.8; the case for which K' was assumed to increase linearly with time, again for first-order reprecipitation kinetics, was considered in Reference 2.9.

Following the procedure developed in Reference 2.8, we express Equation 2-1 in dimensionless form by defining the following:

$$s \equiv C/C_o \qquad (2\text{-}2)$$

$$\tau \equiv KSt/V \qquad (2\text{-}3)$$

$$r \equiv C_o'/C_o \qquad (2\text{-}4)$$

$$\beta \equiv \frac{K'V\,C_o}{KS} \qquad (2\text{-}5)$$

In these terms, Equation 2-1 becomes

$$\frac{ds}{d\tau} = 1 - s - \beta(r-s)^2 \qquad (2\text{-}6)$$

with this equation being valid for $r \leq s \leq 1$. The definitions of s, τ, and r are the same as those used earlier[2.8], with the definition of β being modified somewhat from its prior form[2.8] to account for the second-order kinetics.

One can readily show that the solution of Equation 2-6 can be expressed as follows:

$$s = r + \frac{1}{2\beta}\left\{-1 + \lambda \tanh\left[\frac{\lambda}{2}(\tau - \tau_p) + \tanh^{-1}\left(\frac{1}{\lambda}\right)\right]\right\} \qquad (2\text{-}7)$$

where

$$\lambda \equiv [1 + 4\beta\,(1-r)]^{1/2} \qquad (2\text{-}8)$$

$$\tau_p \equiv \ln\left(\frac{1}{1-r}\right) . \qquad (2\text{-}9)$$

Equation 2-7 is valid for $\tau > \tau_p$ (for which $r \leq s \leq 1$), the definition of τ_p being consistent with that used in Reference 2.8. At least in a qualitative sense, the variation of s with τ, as predicted from Equation 2-7, is similar to that obtained from the model based on first-order reprecipitation kinetics (Equation 2-24 of Reference 2.8). In other words, s rises monotonically from its value of r at time τ_p and asymptotically approaches the value s=1.

2.3.2 Application to Glass-Dissolution Experiment

To apply the above analysis to the data obtained from the glass-dissolution experiment, it is first convenient to alter the form of the effective rate-constant K', as was done previously[2.12] for the case of first-order reprecipitation kinetics. For the reasons already cited[2.12], the effective rate-constant for this particular experiment is proportional to S/V, in which case we define

$$K' = K'' S/(C_0 V) \qquad (2\text{-}10)$$

where K" is another effective rate-constant, but one that is independent of S/V. (The C_0 factor in Equation 2-10 is arbitrarily included simply to make K and K" have the same units.) Upon combining Equations 2-5 and 2-10, we find that the parameter β has the simpler form

$$\beta = K''/K . \qquad (2\text{-}11)$$

Other than this, the analysis presented above remains unchanged. Clearly, with this new form for K', the right-hand side of Equation 2-8 is independent of S/V, so that, as with the case for first-order reprecipitation kinetics, the extent of glass dissolution and precipitate growth is uniquely determined by the magnitude of the parameter St/V.

Equation 2-7 was fitted to the experimental data by again assuming $r \simeq 0$ and using known values for C_0 and S/V. Qualitatively, the fit obtained was similar to that obtained previously based on first-order reprecipitation kinetics. In a quantitative sense, the fit was actually somewhat better for the case of first-order reprecipitation kinetics, as measured by the respective sums of squares of deviations of the data about the fitted curve for the two cases.

Comparison of second-order kinetics to first-order kinetics will continue next quarter.

2.4 References for Section 2

(2.1) M. A. Molecke, "A Comparison of Brines Relevant to Nuclear Waste Experimentation", SAND83-0516 (1983).

(2.2) A. E. Ogard and J. Kerrisk, "Groundwater Chemistry Along Flow Paths Between a Proposed Repository Site and the Accessible Environment", LA-10188-MS (November, 1984) Tables I and II.

(2.3) T. E. Jones, "Reference Material Chemistry--Synthetic Groundwater Formulation", RHO-BW-ST-37P (April, 1982).

(2.4) C. M. Jantzen, "Methods of Simulating Low Redox Potential (Eh) for a Basalt Repository", DP-MS-83-59, prepared by Savannah River Laboratory for the U.S. Department of Energy (1983).

(2.5) A. H. Booth, "A Method for Calculating Fission Gas Diffusion From UO_2 Fuel and Its Application to the X-2-f Loop Test", CRDC-721 (September, 1957).

(2.6) A. H. Booth and G. T. Rymer, "Determination of the Diffusion Constant of Fission Xenon in UO_2 Crystals and Sintered Compacts", AECL-692 (August, 1958).

(2.7) J. Rest, "The Prediction of Transient Fission-Gas Release and Fuel Microcracking Under Severe Core-Accident Conditions", Nucl. Technol. 56 (1981) 553.

(2.8) "Long-Term Performance of Materials Used for High-Level Waste Packaging", D. Stahl and N. E. Miller (Compilers), NUREG/CR-3427, Vol 4, BMI-2113 (June, 1984), pp 2-58 ff.

(2.9) "Long-Term Performance of Materials Used for High-Level Waste Packaging", D. Stahl and N. E. Miller (Compilers), NUREG/CR-3900, Vol. 4, BMI-2127 (July, 1985), pp 2-26 ff.

(2.10) H. H. Hohmann and M. Kahlweit, "Ostwald Ripening of Crystalline Precipitates in Aqueous Solutions at Constant Temperature and Periodic Temperature Changes", Ber. Bunsenges. Phys. Chem. 76 (1972), 933.

(2.11) R. Reich and M. Kahlweit, "Zur Kinetik des Kristallwachstums in Wassrigen Losungen. I", Ber. Bunsenges. Phys. Chem. 72 (1968), 66.

(2.12) "Long-Term Performance of Materials Used for High-Level Waste Packaging", D. Stahl and N. E. Miller (Compilers), last quarterly.

3. OVERPACK CORROSION

During this year, the overpack corrosion studies have focused on the carbon steel-basalt system, although it is recognized that other repositories have equal or greater probability of being licensed. By focusing the research in this fashion, the inefficiencies associated with frequent switching from system to system are minimized. Moreover, many of the methodologies developed in the program and some of the data obtained are applicable to other repository systems. The three continuing overpack corrosion tasks include potentiodynamic polarization studies, slow strain rate studies, and pitting-kinetics studies. The objective of these tasks is to investigate the localized corrosion behavior of carbon steel in repository environments.

Corrosion modeling studies are continuing with current emphasis on enhancing the general-corrosion model and developing a pitting-corrosion model. Basic equations to describe the effect of water radiolysis on general corrosion are being evaluated, and a pit-propagation model is being extended to account for the results of previous pitting-kinetics experiments.

3.1 Potentiodynamic Polarization Studies

Potentiodynamic polarization techniques are being used to evaluate the influence of metallurgical and environmental variables on the electrochemical behavior of carbon steels in simulated basalt repository environments. The results of these analyses are then used to assess the tendency for stress-corrosion cracking (SCC) and pitting.

As explained in the Year Three Annual Report[3.1], in the potentiodynamic polarization procedure, the polarity and magnitude of the current flow between a metal specimen and an inert counter electrode are measured as a function of electrochemical potential. A polarization curve is plotted as the logarithm of net current density versus the electrochemical potential. For the anodic portions of the curve, the current measured is equal to the corrosion rate of the specimen if two conditions are met: (1) the over potential (difference between the free-corrosion potential and the polarized potential) is large enough such that the rates of the cathodic reactions are negligible, and (2) the rates of parasitic oxidation reactions are negligible.

A schematic of anodic polarization curves showing several types of behavior are given in Figure 3.1. For the active-corrosion case, the anodic curve is linear on a potential vs. logarithm of current (E-log i) plot, and the forward and reverse scans are coincident. The presence of a peak in the anodic portion of the curve followed by a decrease in current with increasing potential, generally indicates the onset of passivation. The occurrence of hysteresis between the forward and reverse scans indicates pitting. Where the hysteresis loop is very large, the protection potential may be very close to the open-circuit potential, indicating a high probability of pitting in service.

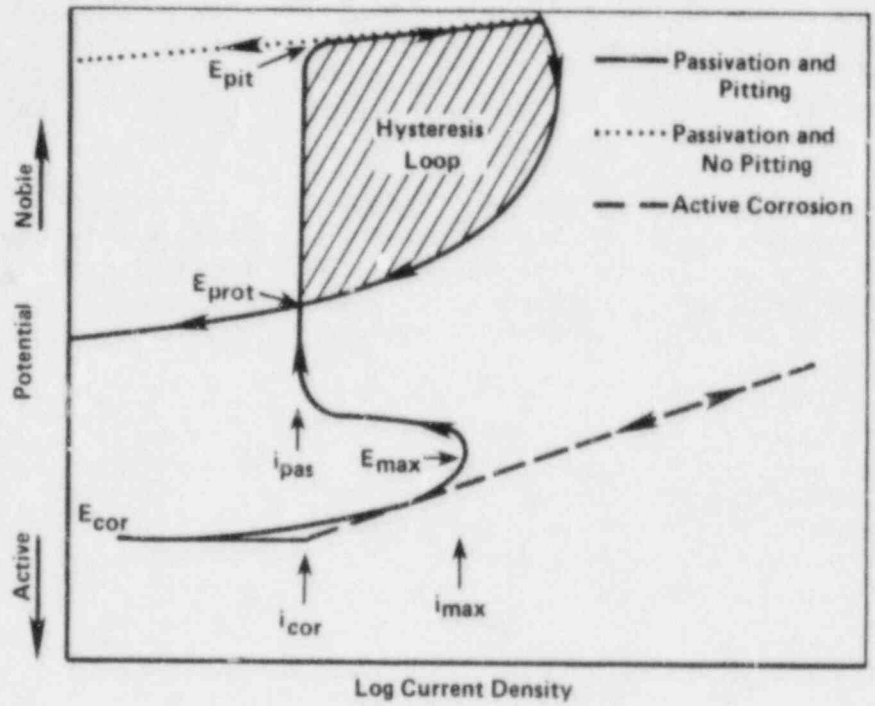

Figure 3.1. Schematic of typical anodic potentiodynamic polarization curves.

E_{cor} = corrosion potential; E_{pit} = potential at which pits initiate on forward scan; E_{prot} = potential at which pits repassivate on reverse scan; i_{cor} = current density at the free-corrosion potential; i_{max} = current density at active peak; i_{pas} = current density in passive range.

The potentiodynamic polarization technique also has been found to be useful in identifying possible SCC environments for carbon steels. It has been shown[3.2] that SCC is associated with environments that promote active-passive behavior and that the range of electrochemical potentials that promotes SCC is near to and more noble (positive) than E_{max} (see Figure 3.1). Moreover, it has been observed[3.2] that severe cracking occurs in environments when i_{max} on the fast scan is greater than about 1×10^{-3} A/cm^2 and where the fast scan exhibits at least an order-of-magnitude higher current than the slow scan.

The polarization behavior of the candidate alloys is being determined using conventional polarization techniques. The equipment used for these experiments includes a PAR Model 173 potentiostat with an ECO Model 567 function generator, coupled to a computer data-acquisition system. A three-compartment electrochemical cell is used that contains a saturated calomel reference electrode (SCE) and a platinum counter electrode. The three-compartment electrochemical cell separates the working electrode from the counter electrode, thus preventing the solutions in the electrode compartments from mixing.

The working-electrode specimens, made from hot-rolled 1020 carbon steel, are cylindrical rods that are axially drilled and tapped. The specimens are mounted on a threaded carbon steel rod with the ends of the specimens sealed from exposure to the cell solution by polytetrafluoroethylene (PTFE) gaskets. The composition of the steel is given in Table 3.1. The specimens are 0.6 cm in diameter and 1.9 cm in length; the actual area of each specimen is measured prior to immersion in the electrochemical cell. The electrodes are polished with successively finer grades of silicon carbide paper, finishing with a 600-grit paper.

Prior to testing, the working electrode remains in the test solution overnight while the solution is sparged with the desired gas mixture. The polarization scans are then started approximately 16 hours after the working electrode is immersed in the cell. Partial cathodic and full anodic polarization curves are obtained by scanning at a rate of 0.6 V/hr and beginning the scan approximately 100 mV more negative than the free-corrosion potential. The current for the anodic curve is scanned until a current density of approximately 3×10^{-3} A/cm^2 is attained; the anodic scan is then reversed until repassivation occurs and the current changes polarity, becoming cathodic. When the polarization plot is completed, a new steel specimen is inserted into the polarization cell containing the same solution and is immediately polarized to a potential of approximately -0.90 V (SCE). Within five minutes of immersion, a fast anodic scan is performed using a scan rate of 18 V/hr. After the polarization scans are completed, the following polarization parameters are obtained from the polarization curves of potential (E) versus logarithm of current density (log i), i_{cor}, E_{cor}, i_{pas}, E_{pit}, E_{prot}, and i_{max} (i_{max} obtained from the fast-scan curve).

As described in the Year Three Annual Report,[3.1] a statistical experimental design approach is being used to evaluate the influence of

Table 3.1. Chemical compositions and other data on steels used in the corrosion studies.

SAE Number or Designation	Thermomechanical Treatment	Tests Used In	Dimensions	Composition (weight percent)										
				C	Mn	P	S	Si	Cu	Sn	Ni	Cr	Mo	Al
1018	Hot-Rolled	Pitting Exposures	7.6 cm x 15.2 cm strip	0.18	0.77	0.017	0.019	0.22	--	--	--	--	--	--
1020[a]	Hot-Rolled	Electrochemical Pitting Monitor, Potentiodynamic Polarization	1.27 cm rod	0.20	0.46	0.011	0.032	0.17	0.38	0.027	0.014	0.018	0.024	--
1020[a]	Hot-Rolled	Slow Strain Rate	0.635 cm dia. rod	0.22	0.55	0.01	0.037	--	--	--	--	--	--	--
Clean BCL Steel	Cast or Hot-Rolled	Potentiodynamic Polarization	Ingot	0.18	0.49	0.004	0.002	0.30	0.006	--	0.002	0.007	0.00	0.10
Doped BCL Steel	Cast or Hot-Rolled	Potentiodynamic Polarization	Ingot	0.17	0.55	0.029	0.036	0.35	0.007	--	0.004	0.011	0.00	0.14
Ferrovac E	Cast	Potentiodynamic Polarization	Ingot	0.003	Tr[b]	--	--	Tr	--	--	Nil[c]	Nil	Tr	Nil

(a)Hot-rolled 1018 carbon steel not available in rod form.
(b)Tr = Trace.
(c)Nil = None detected.

environmental variables on the electrochemical behavior of carbon steel in simulated repository environments. The statistical analysis performed and presented in the Year Three Annual Report used the design values for the chemical concentrations of the eleven control variables. Because of solubility considerations and interaction among variables, e.g., most notably pH/CO_3^{-2}/HCO_3^-, the design concentrations of the variables were not realized. Therefore, part of Year Four work involved analyzing the actual concentrations of the elements present in the solutions for the experiments previously performed.

During the polarization experiments in Year Three, solution samples were collected from each experiment. As part of the collection procedure, a filtering process was used to remove any precipitate present in the test solution. Therefore, the sample consisted of only the dissolved species present at the time the test was performed. Prior to analysis, any precipitates that formed during storage of the samples were redissolved, so that the analyses performed provided elemental concentrations representative of those present in solution at the time of testing.

The statistical analysis that was described in the Year Three report was then repeated, using the actual concentrations of the species in solution, rather than the design concentrations. The analyses of the data are still in progress, but the results of the regression analyses are presented in Tables 3.2 and 3.3.

Table 3.2 shows the main-effect terms at a 90 percent probability of significance level. The arrows indicate the direction of the regression coefficient. The table compares the results of the regression analysis for the designed chemical data (Year Three Report) to the regression analysis for the analyzed chemical data. The measured concentrations of some of the variables were significantly different from the designed concentrations, e.g., for Si, Fe, F, and CO_3/HCO_3, so it is not surprising that the regression results were altered. Several new effects were observed and some effects were dropped with the new analysis. However, the main effects which showed up in both analyses had the same direction with the exception of E_{pit} and E_{prot} for pH and E_{pit} for NO_3/NO_2. In all cases, the new analysis, which used the analyzed solution concentrations, is believed to give the more reliable prediction of the true effects of the species on corrosion.

Table 3.3 shows a similar comparison for the two-factor interaction terms. As for the main-effect terms, several new effects were identified when the analyzed solution concentrations were used. The only contradictions when both analyses showed the same effect were for E_{pit} and E_{prot} for the pH x CO_3 interaction and E_{cor} for the SiO_3 x O_2 interaction. Also, three interaction terms were indicated as having several effects on the corrosion parameters which did not show up in the previous analysis; these were pH x SiO_3, pH x CO, and NO_3 x SiO_3.

The statistical analysis of the data is proceeding, and refinements to the analysis may result in the removal of some of the reported effects

Table 3.2. Summary of main-effect terms for main matrix comparing the statistical results based on designed chemical data with those based on analyzed chemical data.[a]

	E_{cor}	log i_{cor}	log i_{max}	log i_{pas}	E_{pit}	E_{prot}
pH	- -	↓ ↓	↓ ↓	↓ ↓	↓ ↑	↓ |
Cl	↓ ↓	- -	↓ ↓	- ↑	- ↓	↓ ↓
F	↓ -	↑ -	↑ ↑	↑ -	↓ -	↓ -
Fe	↓ -	- -	↑ -	- -	- -	- -
CO_3/HCO_3	↓ ↓	↑ -	↑ ↑	- -	↑ ↑	↑ -
NO_3/NO_2	↑ ↑	↓ ↓	- -	- -	↓ ↑	- -
BO_3/B_4O_7	- -	- -	- -	- -	- ↑	↑ ↑
SiO_3	↑ -	- ↓	- -	- ↓	↑ -	↑ -
H_2O_2	- -	↑ ↑	- -	- ↑	- -	- -
O_2	- ↑	- -	- -	- -	↑ ↑	- -
CO	- -	- -	↓ -	- -	- -	- -

(a) ↑ or ↓ : increase or decrease, respectively, in response parameter (E_{cor}, etc.) resulting from increase in control parameter (pH, Cl, etc.) for main matrix with designed chemical data .

↑ or ↓ : increase or decrease, respectively, in response parameter resulting from increase in control parameter for main matrix with analyzed chemical data.

-- : indicates that no effect was observed.

Table 3.3. Summary for two-factor interactions comparing the statistical results based on designed chemical data with those based on analyzed chemical data.(a)

	E_{cor}		log i_{cor}		log i_{max}		log i_{pas}		E_{pit}		E_{prot}	
pHxCl	↓	↓	-	↑	↑	↑	-	-	↓	-	↓	↓
pHxCO_3	↑	↑	↓	-	↓	-	-	-	↓	↑	↓	↑
pHxNO_3	↓	↓	-	-	-	-	↓	-	-	-	-	-
pHxBO_3	↓	-	-	-	-	↓	-	↓	-	↓	-	-
pHxSiO_3	↓	-	-	-	-	-	↓	-	↓	-	↓	-
pHxH_2O_2	-	-	↓	-	↓	-	-	-	-	-	-	-
pHxO_2	-	-	↑	-	-	-	↑	-	↓	↓	↓	↓
pHxCO	-	-	↓	-	↓	-	-	-	↓	-	↓	-
ClxCO_3	↑	↑	-	↓	↓	-	↓	↓	↑	↑	-	-
ClxNO_3	-	-	↑	↑	-	-	↑	↑	-	-	↑	-
ClxBO_3	-	-	-	-	-	↓	↓	↓	↓	↓	↓	↓
ClxH_2O_2	↓	-	-	-	↓	↓	↓	↓	-	-	-	-
CO_3xH_2O_2	↓	↓	-	-	-	-	-	-	-	-	-	-
CO_3xO_2	-	-	-	-	-	-	-	-	-	-	-	-
NO_2xBO_3	-	-	-	-	-	-	-	-	-	-	-	-
NO_3xSiO_3	↓	-	↓	-	↓	-	↓	-	↓	-	-	-
NO_3xO_2	-	-	↑	↑	-	↑	↑	↑	-	↑	↑	↑
BO_2xSiO_3	-	-	-	-	-	-	-	-	-	-	↓	↓
BO_2xH_2O_2	-	-	↓	↓	-	-	-	-	-	-	-	-
SiO_3xO_2	↓	↑	-	-	-	-	-	↓	-	-	-	-
H_2O_2xO_2	↓	↓	-	-	-	-	-	-	↓	-	-	-

(a) ↑ or ↓ : increase or decrease, respectively, in response parameter (E_{cor}, etc.) resulting from increase in control parameter (pH, Cl, etc.) for main matrix with designed chemical data.

↑ or ↓ : increase or decrease, respectively, in response parameter resulting from increase in control parameter for main matrix with analyzed chemical data.

-- : indicates that no effect was observed.

in the final model to be outlined in the Year Four Annual Report. A large portion of the analysis yet to be completed involves considering the correlations that resulted from not meeting the designed concentrations. The experimental design initially represented very low correlations among all of the effects being considered. Because these designed concentrations were not met, some correlations among effects occurred. These possible correlations will be considered during further analyses in the fourth quarter of Year Four research.

When the final analyses are completed, the results of the potentiodynamic polarization studies will be used to predict species and interactions of species that are especially deleterious to the localized corrosion behavior of carbon steel in a repository. These data will then be used to guide future research in which localized corrosion in these deleterious environments will be investigated in greater detail. As described in other sections, some of these experiments have been started or are planned for the near future. That a given environment is deleterious must be established through independent laboratory, field, and modeling studies of the repository geohydrology.

3.2 Slow Strain Rate Studies

Slow strain rate experiments on selected environments from the potentiodynamic polarization studies were planned for this reporting period, but these experiments were deferred until the first quarter of the next program year to concentrate resources on the pit-propagation experiments.

3.3 Pitting-Kinetics Studies

Results of the potentiodynamic polarization experiments and autoclave exposures performed in Year Two suggested that pit initiation in low-carbon steels is likely in basalt groundwater. The polarization curves exhibit considerable hysteresis on the reverse scans, and protection potentials are very near the corrosion potentials, even for deaerated solutions. In the autoclave exposures, pits actually were found on specimens exposed for approximately 1000 hours in a deaerated simulated basalt groundwater at 250 C.

Accordingly, experiments were undertaken to characterize the pit-propagation behavior of carbon steel in simulated basalt-repository environments. Two types of experiments are being performed: weight-loss experiments and electrochemical pit-propagation experiments. The objective of these experiments is to characterize the pit-propagation behavior of carbon steel in simulated repository environments and to develop an understanding of the mechanism of attack. Results of experiments performed this reporting period are discussed below.

3.3.1 Electrochemical Pit-Propagation Experiments

A schematic of the pit-propagation monitor is shown in Figure 3.2. Experimentally, the monitor is positioned vertically in a test cell

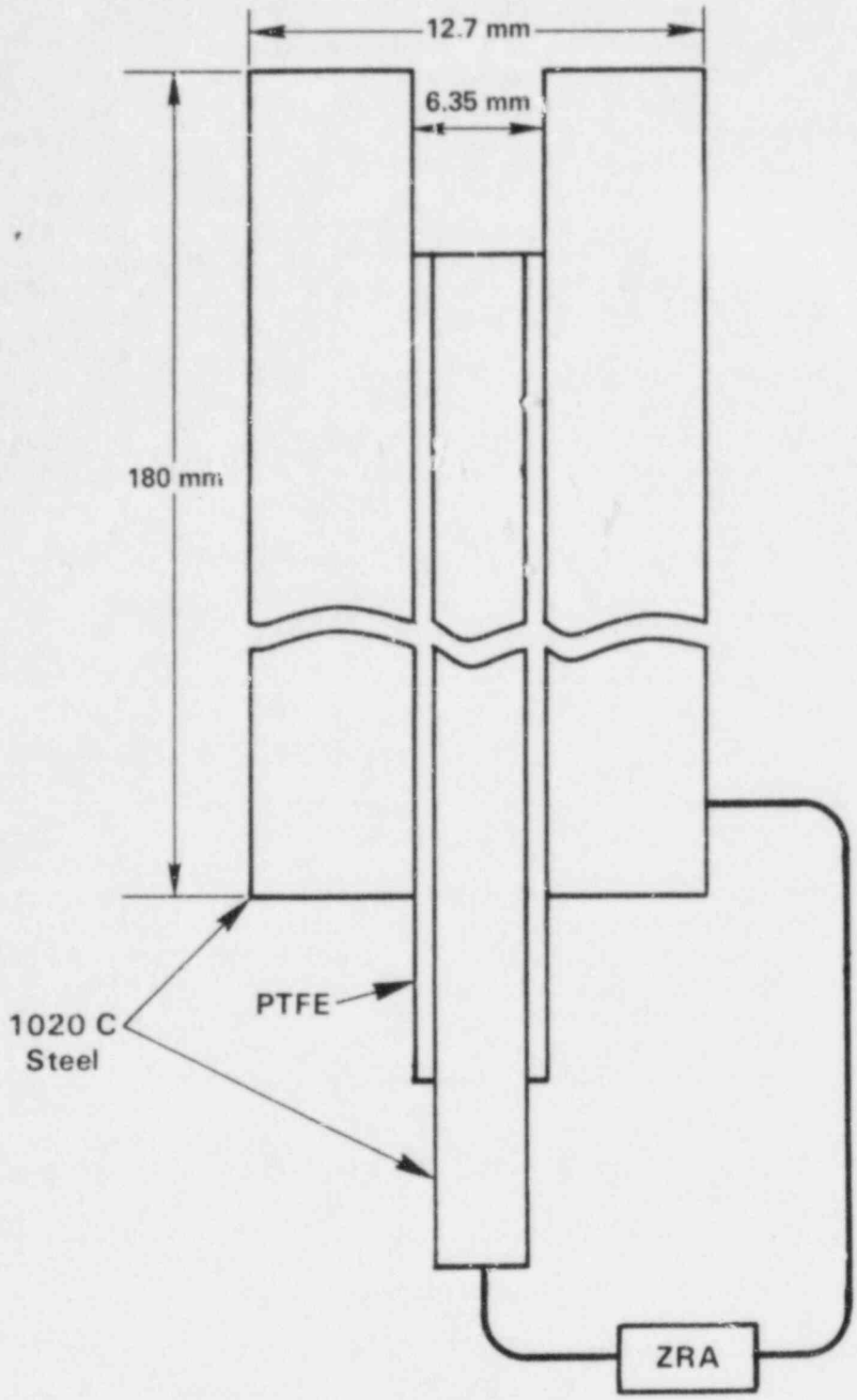

ZRA = Zero Resistance Ammeter

Figure 3.2. Schematic of pit-propagation monitor.

containing an electrolyte, and the current flow between the base of the simulated pit and the boldly exposed surface (BES) is monitored as a function of exposure time. Current measurements provide an estimation of the rate of pit propagation where shifts in the electrochemical potential of the pit base, as a result of the couple, are greater than about 50 mV. For potential shifts less than this value, the rate measured may be somewhat non-conservative since the reduction reactions occurring on the pit base will contribute to pit propagation but will not be detected.

A standard procedure has been developed to initiate pitting with the monitor. This procedure consisted of (1) pre-packing the simulated pit with a paste prepared with an electrolyte and Fe_3O_4, (2) deaerating the test solution for 24 hours to fully deaerate the pit, during which time the simulated pit and boldly exposed surfaces are not coupled, and (3) aerating the test solution and coupling the simulated pit and boldly exposed surface through the zero-resistance ammeter (ZRA).

Double-walled PYREX* cells are used in the experiments so that the temperature can be controlled by flowing a heat-transfer solution in the annular region between the inner and outer walls. The cells consist of (1) a counter electrode cell containing a platinum electrode for potentiodynamic or potentiostatic measurements, (2) a reference electrode cell containing a saturated calomel electrode (SCE) for electrochemical potential measurements, (3) a platinum wire for Eh measurements, (4) a frit bubbler for deaeration or aeration of the solution, and (5) provisions for refreshing the solution continuously. Prior to the test, the specimens are cleaned with acetone and assembled, and the simulated pits are packed with a paste as previously described. The specimens are then inserted in the cell, the test solution is added, and the experiment is started. During the course of the experiment, coupled potentials, Eh, temperature, and galvanic current flow are continuously monitored and recorded with a data acquisition system. Solution and gas flow rates are continuously monitored and maintained at 40 cc/hour and 10 cc/min, respectively.

During Year Three, it was found that the simulated pits passivated during the course of the experiments when they were packed with a basalt groundwater -Fe_3O_4 paste. It was thought that this passivation led to non-conservative estimates of the rate of pit propagation; accordingly, experiments were carried out to attempt to activate the pits.

The pits were packed with acidified Fe_3O_4 pastes, prepared with 0.1 N** or 0.01 N HCl and Fe_3O_4 rather than with basalt groundwater and Fe_3O_4. The results of the electrochemical measurements performed on these pits

---

* PYREX is a registered trademark of Corning Glass Works.
** N = Normal.

indicated that the 0.1 N HCl-packed pit was clearly active, but the measured ZRA currents were low and comparable to those measured for the pits which were packed with the less-aggressive electrolytes. On the other hand, results of analysis of the polarization curves* performed on the pits following one week of propagation indicated that the corrosion rates of the pit bases were one to two orders of magnitude higher than the corrosion rates estimated from the ZRA measurements. In addition, the coupled potentials, for the pit--boldly exposed surface couple, measured during the pit-propagation experiments, were very close (within 5 mV) to the free-corrosion potentials measured for the pit bases prior to obtaining potentiodynamic polarization curves. It was speculated from these observations that the reduction reactions occurring within the pit, and not the galvanic (ZRA) currents, were the primary contributors to corrosion attack of the pit bases.

Experiments were performed last quarter to test this hypothesis. The pit-propagation experiments with acidified packing pastes were repeated with the addition of careful weight-loss measurements on the pit bases and instant-off potential measurements on the pit bases and boldly exposed surfaces. In the latter measurements, the ZRA current was interrupted periodically during the course of the experiments and the potentials of the pit base and boldly exposed surfaces were then measured, with respect to a calomel reference electrode. By interrupting the current, the potential (IR) drop down the pit associated with current flow between the pit base and the BES specimen was eliminated.

Results of the experiments confirmed the hypothesis that the reduction reactions within the pit control the corrosion rate of the pit. The weight losses on the pit bases were over an order of magnitude higher than the values estimated from the ZRA currents, and the instant-off potentials for the pit bases were within a few millivolts of the potentials of the boldly exposed surfaces.

In summary, the results of the pit-propagation experiments performed last quarter suggest that the electrode kinetics within the pit have a dominant influence on the rate of pit propagation. This conclusion was reached on the basis of results of electrochemical experiments performed on simulated pits having active walls. This geometry was selected for study because it more closely simulates the geometry of actual pits than the geometry used for many electrochemical studies in which the pits have inert walls. The inert-wall geometry is frequently selected for these studies because it simplifies the mathematical modeling. However, since the results of this program are not consistent with transport-limited models that have been developed based on inert-wall pits, pit-propagation experiments were performed this quarter to compare the two geometries.

---

* Tafel Extrapolation.

In the first electrochemical test performed this quarter, the pit-propagation experiments (performed last quarter) were repeated with an inert-wall geometry. As in the previous tests, the experiments were performed at 75 C in basalt groundwater with pits having a diameter-to-depth ratio of 1:5 and with two packing pHs: 0.1 N HCl (Cell A) and 0.01 N HCl (Cell B). As in the previous tests, the current and coupled potential were monitored during the course of the tests, and on a daily basis the pit and BES specimens were uncoupled and their potentials were measured over a 30-minute period. The cells were then recoupled and the current and coupled-potential measurements were resumed.

Results of the current measurements are given in Figures 3.3 and 3.4. As in the previous tests, these data exhibit considerable scatter but the average currents were considerably higher than those measured with the active-wall geometry (reported last quarter).

The most striking difference between the results for the two geometries was in the uncoupled-potential measurements. The data for the inert-wall geometry, which are given in Figure 3.5, show that the uncoupled potentials for the pit and BES specimens were as much as 100 mV apart and averaged over 50 mV for both cells. This is in contrast to the potential data for the active-wall pits where the uncoupled-potential difference between the pit and BES specimen for a given cell was less than 5 mV.

The data in Figure 3.5 also show a potential difference of about 100 mV between Cell A (.01 N HCl package paste) and Cell B (0.1 HCl package paste) for either the BES or the pit specimen in the respective cells. This behavior was found to be the result of a defective reference electrode in Cell B and is thus of no consequence. This finding, however, does not alter the conclusions reached from the data in any way since the pit and BES specimen potentials for each cell were measured with respect to a single reference electrode. Thus, the net displacement of the potential of the calomel electrode affected the absolute value of the potential readings for a given cell but did not alter the potential difference between the pit and the BES for that cell.

In a second short-term electrochemical experiment, stable pitting was established for active-wall and inert-wall pits, and a glass micro-capillary was moved down the pits to measure the effect of pit-wall activity on the potential profiles. These experiments were somewhat different from the previous ones in that they were performed at room temperature and with zirconia packing rather than Fe_3O_4 packing. This was done to minimize an oozing phenomena* that had been noted with experiments performed at elevated temperatures with this paste. As in

---

* In several of the experiments, it was noted that the Fe_3O_4 packing paste expanded and oozed out of the pits during the tests.

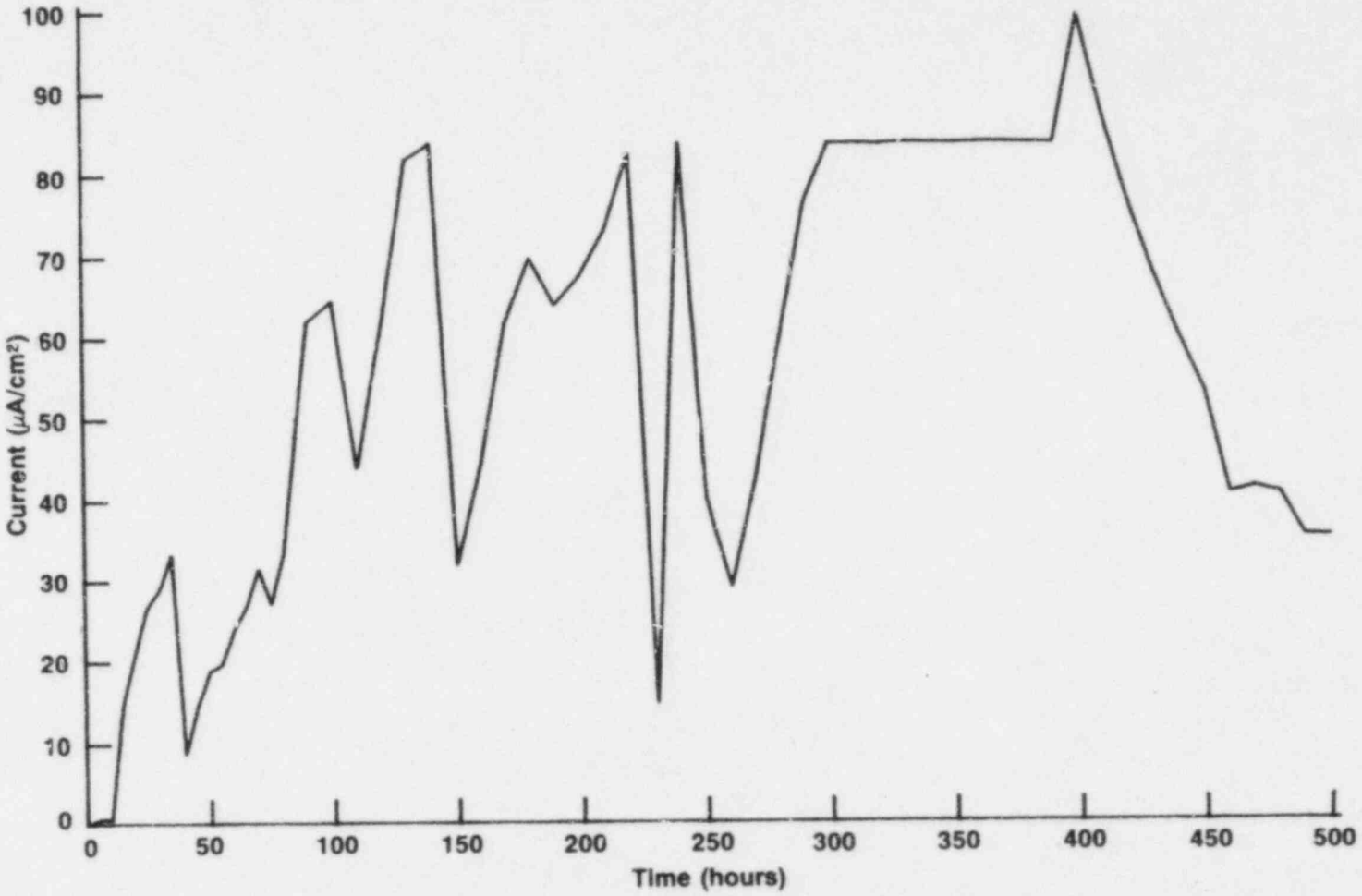

Figure 3.3. Current density as a function of time for experiments performed with inert-wall pits at a diameter-to-depth ratio of 1:5 in aerated basalt groundwater at 75 C with a 0.01 N HCl-Fe_3O_4 paste packing.

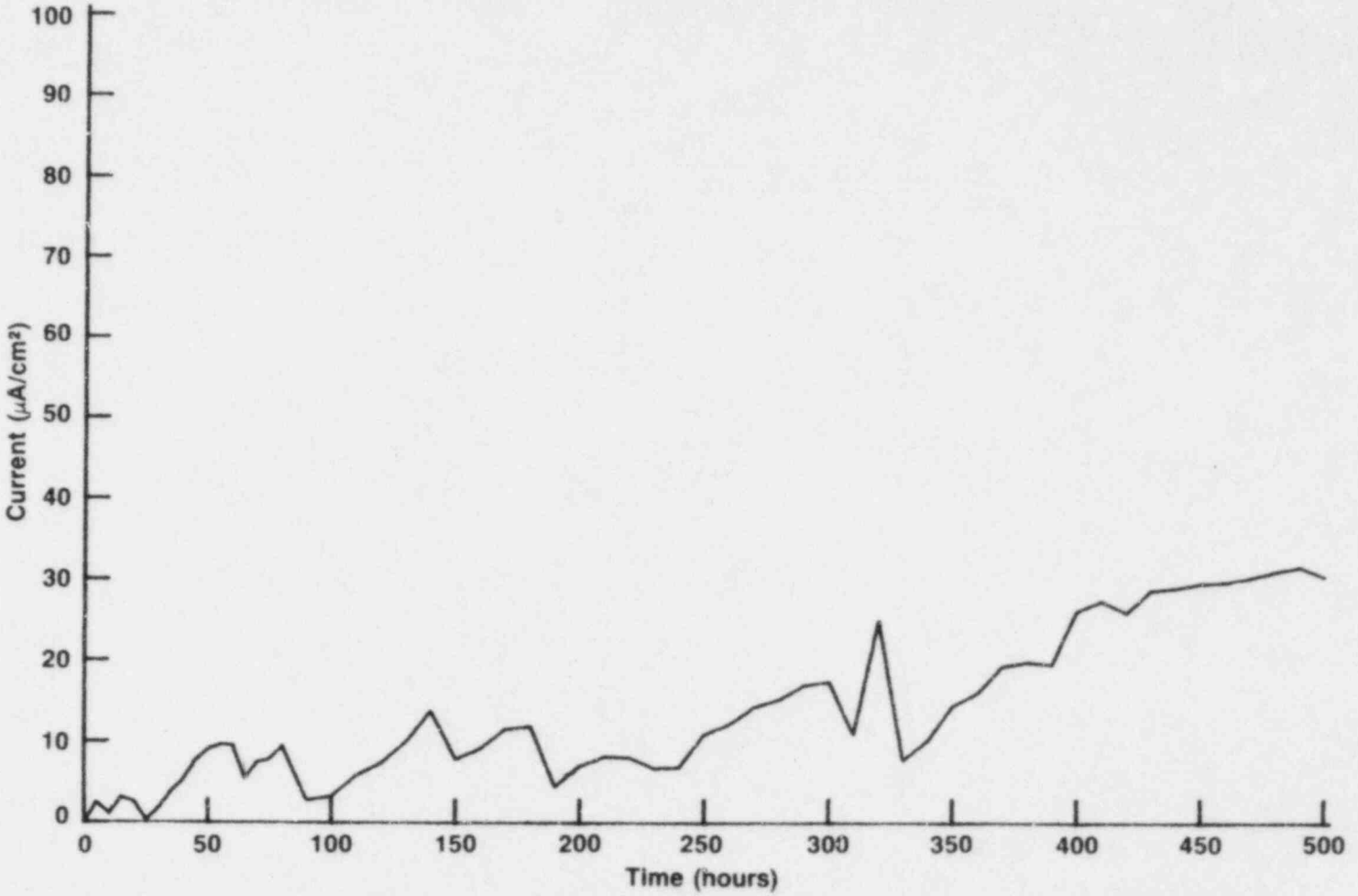

Figure 3.4. Current density as a function of time for experiments performed with inert-wall pits at a diameter-to-depth ratio of 1:5 in aerated basalt groundwater at 75 C with a 0.1 N HCl-Fe_3O_4 paste packing.

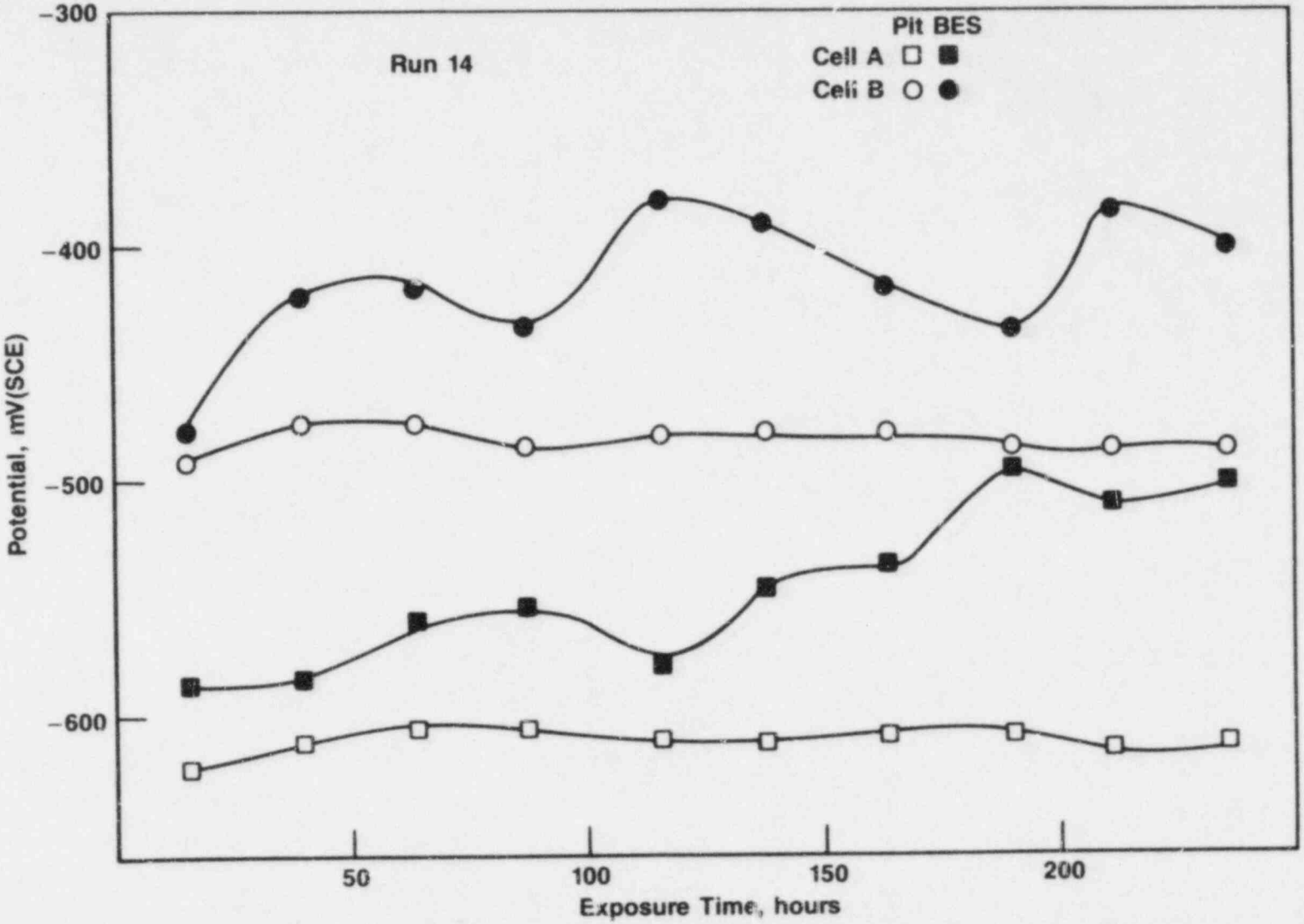

Figure 3.5. Electrochemical potential of the pit and the BES (uncoupled) as a function of exposure time for experiments performed with inert-wall geometry at a diameter-to-depth ratio of 1:5 in oxygenated basalt with 0.01 N HCl (Cell A) and 0.1 N HCl (Cell B) paste-packed pits.

the previous tests, a diameter-to-depth ratio of 1:5 was used and the experiments were performed with basalt groundwater and a 0.1 N HCl packing paste.

The potential measurements were performed with the BES specimen and the pit specimen uncoupled so that no current was flowing from the pit bases. Results of this experiment are given in Figure 3.6. These data show that there was no potential gradient down the inert-wall pit and that, for this pit geometry, there was a significant difference between the potentials of the pit base and the boldly exposed surface. The absence of a potential gradient down the pit indicates that there was no current flow. The large potential difference between the pit base and the BES provides the driving force for pit propagation.

As shown in Figure 3.6, the behavior of the active-wall pit was quite different from the inert-wall pit. There was no apparent driving force for pit propagation as indicated by the similarity of the potential of the BES and pit measured at the pit mouth. On the other hand, a significant potential gradient existed down the pit and was most steep near the pit mouth. Deep within the pit, the potential of the pit base was similar to the uncoupled potential for the inert-wall geometry. The implication of these results for the active-wall geometry is that, in the absence of current flow from the pit base, significant current flow occurs near the pit mouth and creates the high IR drop observed. This effectively shields the pit base from the field of the boldly exposed surface.

During this reporting period, AC impedance experiments also were performed in conjunction with several of the pit-propagation experiments. The objective of these experiments was to obtain an estimate of the resistance down the pits and to evaluate the influence of pit wall activity and other variables on the resistance. The technique also provides information on polarization resistance, which is inversely related to corrosion rate, and on other electrochemical parameters such as the interfacial capacitance.

The experimental technique is simple in concept. A Solartron Model 1250 frequency response analyzer in conjunction with a potentiostat is used to apply a low-amplitude ($\pm$ 20 mV) AC voltage to the specimen, and the magnitude and phase shift of the AC current response is then measured. Measurements are performed over a range of frequencies and the data obtained are analyzed assuming a simple analog electrical model, which is shown in Figure 3.7. The electrical interface is assumed to be a resistance R_p in parallel with a capacitance, C, which are both in series with a solution resistance, R_s. A typical Bode plot, which is a plot of the cell impedance and phase angle as a function of frequency, is given in Figure 3.8 with the values of R_s, R_p, and C indicated. The value of R_s is equal to the value of Z at large values of ω since the series capacitance becomes shorted at high frequencies; $Z_C = 1/j\omega C \rightarrow 0$ as $\omega \rightarrow \infty$. At low frequencies, Z_C becomes very large (as $\omega \rightarrow 0$, $Z_C \rightarrow \infty$) and the total impedance becomes $Z = R_s + R_p$. Therefore, both R_s and R_p are easily determined.

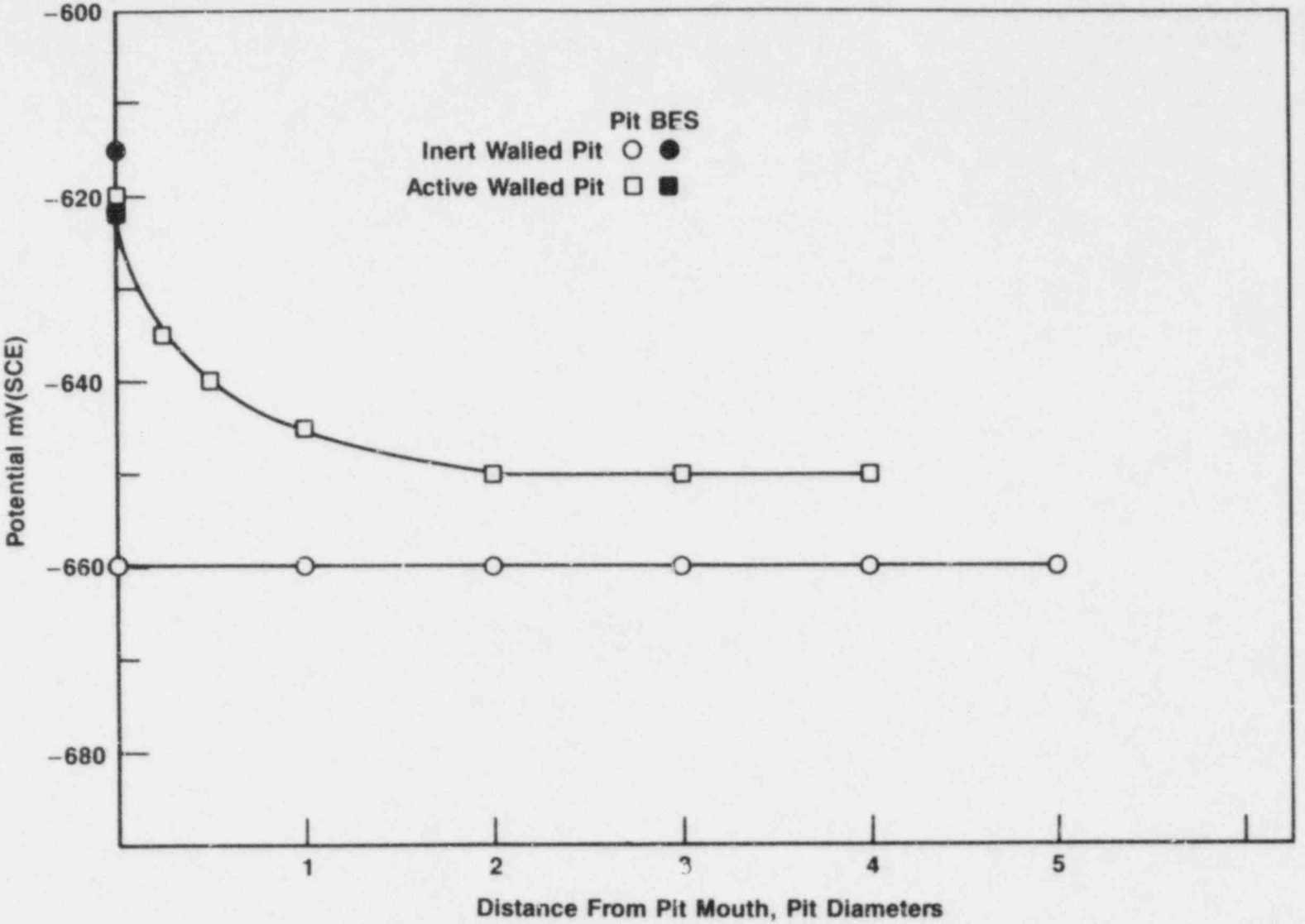

Figure 3.6. Potential of the pit as a function of microcapillary position down pit for uncoupled inert- and active-wall pits.

Potentials for the BES specimens are also given for comparison.

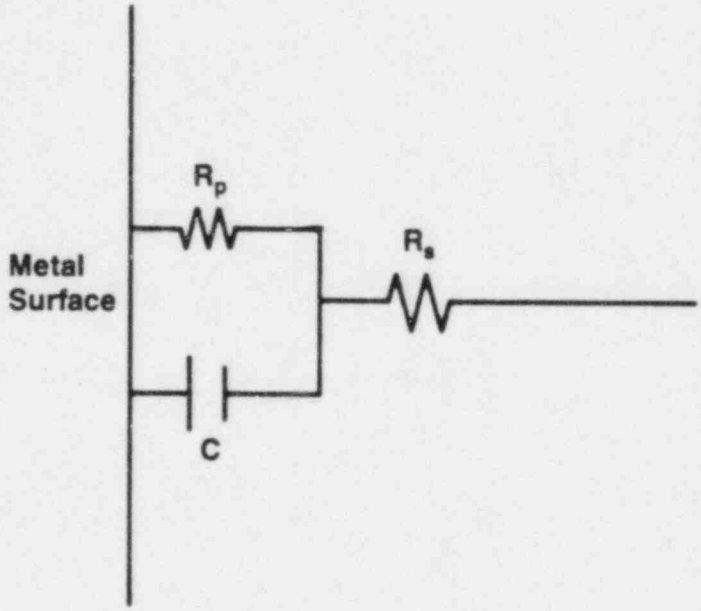

$$z = R_s + \frac{R_p}{1 + R_p J\omega C}$$

Figure 3.7. Analog electrical model used for the AC impedance analysis.

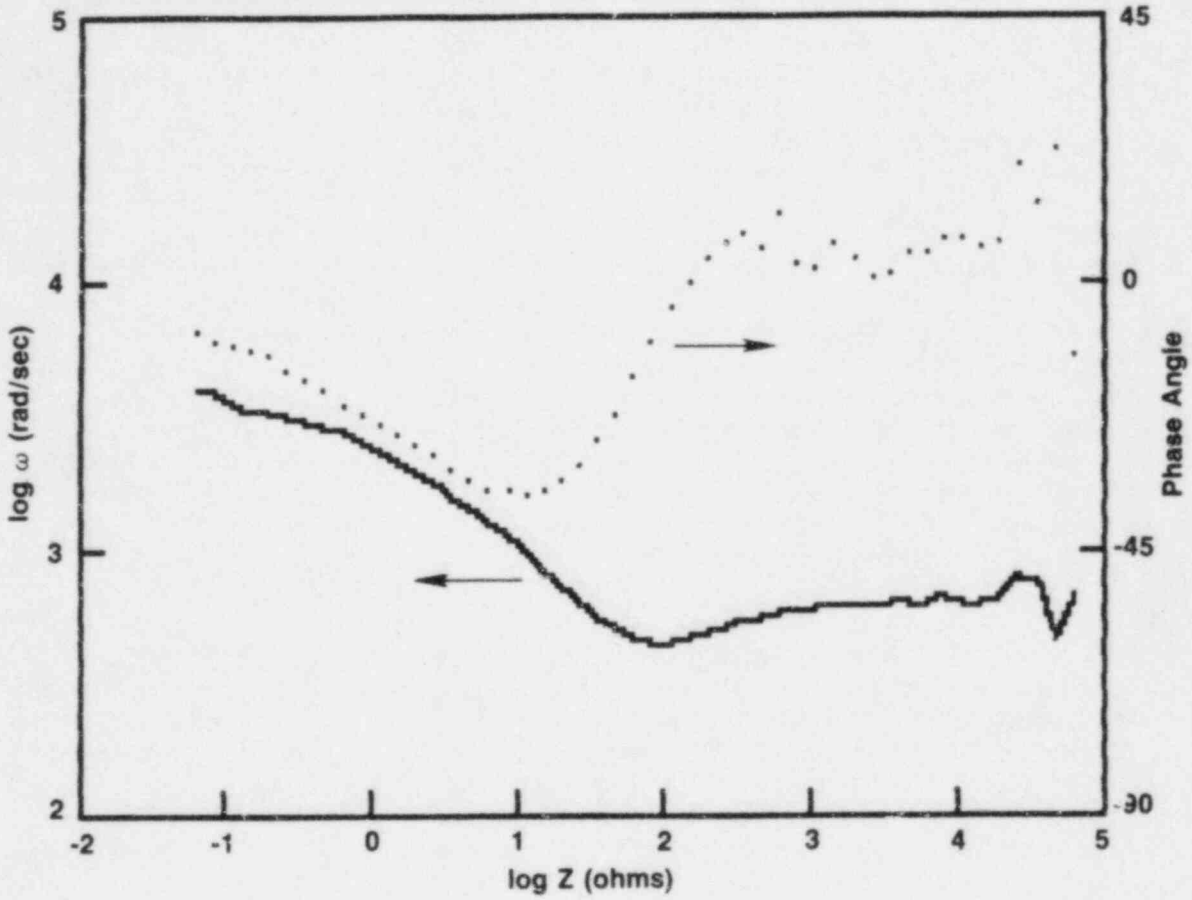

Figure 3.8. Bode plot for the pit on run Number 14A.

The value of the capacitance is somewhat more difficult to calculate. For an ideal system, the slope of the curve between the low and high frequency plateaus is equal to -1, which corresponds to the slope for a pure capacitor;

$$Z = 1/j\omega C \rightarrow \log Z = (-1)\log j\omega C.$$

By extrapolating this line to $\omega = 1$, the value of C can be calculated; $Z_{\omega=1} = 1/C$. In practice, the slope of the curve is rarely -1 and thus a -1 slope is generally extrapolated from the inflection point on the curve to $\omega = 1$ in order to calculate C.

A summary of the AC impedance experiments performed this quarter is given in Table 3.4. Although the data are limited at this time and it is difficult to identify clear trends, several interesting features are noteworthy. First of all, the solution resistance data, R_S, clearly show the highly resistive nature of the pits in comparison to the BES specimens. R_S values for the BES specimens were less than 5 ohms; whereas, R_S values for the pits were 2 to 4 orders of magnitude higher. Thus, the R_S values for the pits represent the resistance down the pits since the R_S values for the BES specimens are extremely low. The data seem to indicate that R_S values are higher for inert-wall pits than for active-wall pits. Significant differences between the data, e.g., ω_ϕ* and C values, for the two sets of experiments, 14 and 15, are apparent and may relate to the different temperatures used for the experiments. As data become available, these trends and their significance will be studied in greater detail.

3.3.2 Weight-Loss Experiments

Weight-loss tests of 1000-hours duration were carried out on simulated pits to aid in interpretation of the electrochemical experiments. Specimens having the same geometry as those used in the electrochemical pit-propagation experiments, but shortened in the axial direction, (see Figure 3.2) were exposed to three environments: a pitting environment, aerated basalt groundwater, and deaerated basalt groundwater at 75 C. The pitting environment was solution Number 47[3.1] from the potentiodynamic polarization task and was selected on the basis of the results of those studies.

Other variables in addition to test solution composition and degree of aeration that were included in the experiments were pit diameter-to-depth ratio (1:1 and 1:2), coupling of the pit to the boldly exposed surface (coupled and uncoupled), and the pH of the Fe_3O_4 paste used to pack the pits (about pH=1 (0.1M HCl) and about pH=2 (0.01M HCl)). The experiments were carried out in a flow-through system with the solution

---

* ω_ϕ = frequency at maximum phase shift.

Table 3.4. Summary of AC impedance data obtained for experiments 14A, 14B, 15A, and 15B.

Run No.	Packing	Packing Normality	Wall	Specimen	R_s (ohms)	R_p (ohms-cm^2)	$\omega\phi$ (Rad/s)	C (μF/cm^2)	Test Temperature
14A	Fe_3O_4	0.01 N	Inert	Pit	2.53×10^3	99	0.064	3.93×10^4	75 C
14A	Fe_3O_4	0.01 N	Inert	BES*	0.79	81	0.068	1.33×10^5	75 C
14B	Fe_3O_4	0.1 N	Inert	Pit	2.58×10^4	304	0.068	4.36×10^3	75 C
14B	Fe_3O_4	0.1 N	Inert	BES	1.39	57	0.066	0.37×10^4	75 C
15A	Zirconia	0.1 N	Act.	Pit	623	447	9.47	653	25 C
15A	Zirconia	0.1 N	Act.	BES	4.02	898	6.11	371	25 C
15B	Zirconia	0.1 N	Inert	Pit	1.37×10^4	1.78×10^3	1.0	349	25 C
15B	Zirconia	0.1 N	Inert	BES	2.93	672	5.65	553	25 C

* Boldly Exposed Surface.

being refreshed twice a week to maintain a constant bulk-solution pH throughout the exposure period.

Results of the weight-loss tests for the three environments are given in Figures 3.9 to 3.11. Figure 3.9, which contains data for the deaerated basalt groundwater, shows that the BES specimens had, in general, very low corrosion rates in this environment, 25 to 50 μm/yr, which were not affected by pit diameter-to-depth ratio or packing pH. The corrosion rates of the BES specimens appeared to be slightly lower for the coupled than for the uncoupled condition, as one might expect, but the differences were small.

The corrosion rates for the pits were generally higher than for the BES specimens (200 μm/yr versus 25 to 50 μm/yr) but, nevertheless, were moderate. There was no systematic effect of pH, coupling, or diameter-to-depth ratio on the corrosion rate of the pits. Thus, in the deaerated basalt groundwater, the corrosion rates of the pits were moderate and were probably controlled by the environment that developed within the pits.

Results of the weight-loss experiments performed in the aerated basalt groundwater are given in Figure 3.10, where it can be seen that the corrosion rates for the boldly exposed surfaces were quite high, about 500 μm/yr, and that there was considerable scatter in the data. Optical examination of the BES specimens indicated that the high corrosion rates were the result of occluded cell corrosion occurring beneath deposits. The data in Figure 3.11 also show that uncoupled corrosion rates for the pits were comparable to the corrosion rates for the BES specimens, whereas coupled corrosion rates for the pits were considerably higher than corrosion rates for the respective BES specimens at a diameter-to-depth ratio of 1:1. This coupling effect appeared to drop off rapidly with increasing pit depth; for the 1:2 diameter-to-depth ratio pit, the effect of coupling on the corrosion of the pits was much less pronounced.

The corrosion data for the aerated pitting solution are given in Figure 3.11. These data exhibit much less scatter than that observed for the aerated basalt groundwater but, nevertheless, the trends in the data were similar. Coupling clearly accelerated the rate of attack of the pit, and the effect of coupling dropped off rapidly with increasing diameter-to-depth ratio. Corrosion rates shown in Figure 3.11 for the BES specimens were extremely low, indicating that the pitting solution effectively passivated the surfaces of these specimens. The data in Figure 3.11 also indicate that the packing pH did not have an effect on the corrosion behavior of either the pit or the BES specimens.

To investigate the effect of the diameter-to-depth ratio of the pit and the relationship between pit-wall activity (inert versus active wall) on pitting rates, another matrix of 1000-hour exposures was performed. These tests were performed with a single packing with a pH of 1 in the aerated pitting solution. The previous tests did not indicate a large

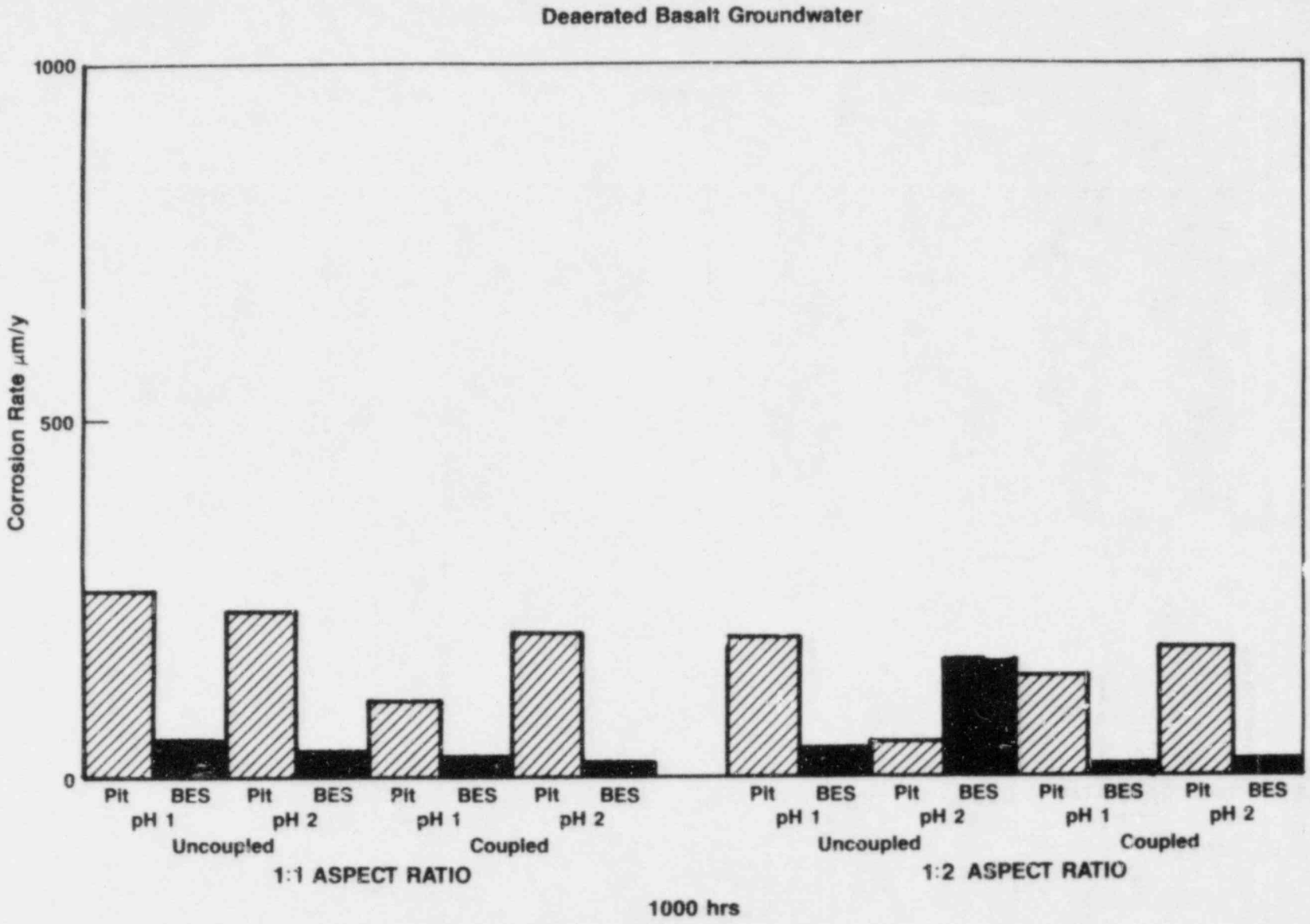

Figure 3.9. Results of 1000-hour weight-loss tests performed on simulated pits in deaerated basalt groundwater at 90 C.

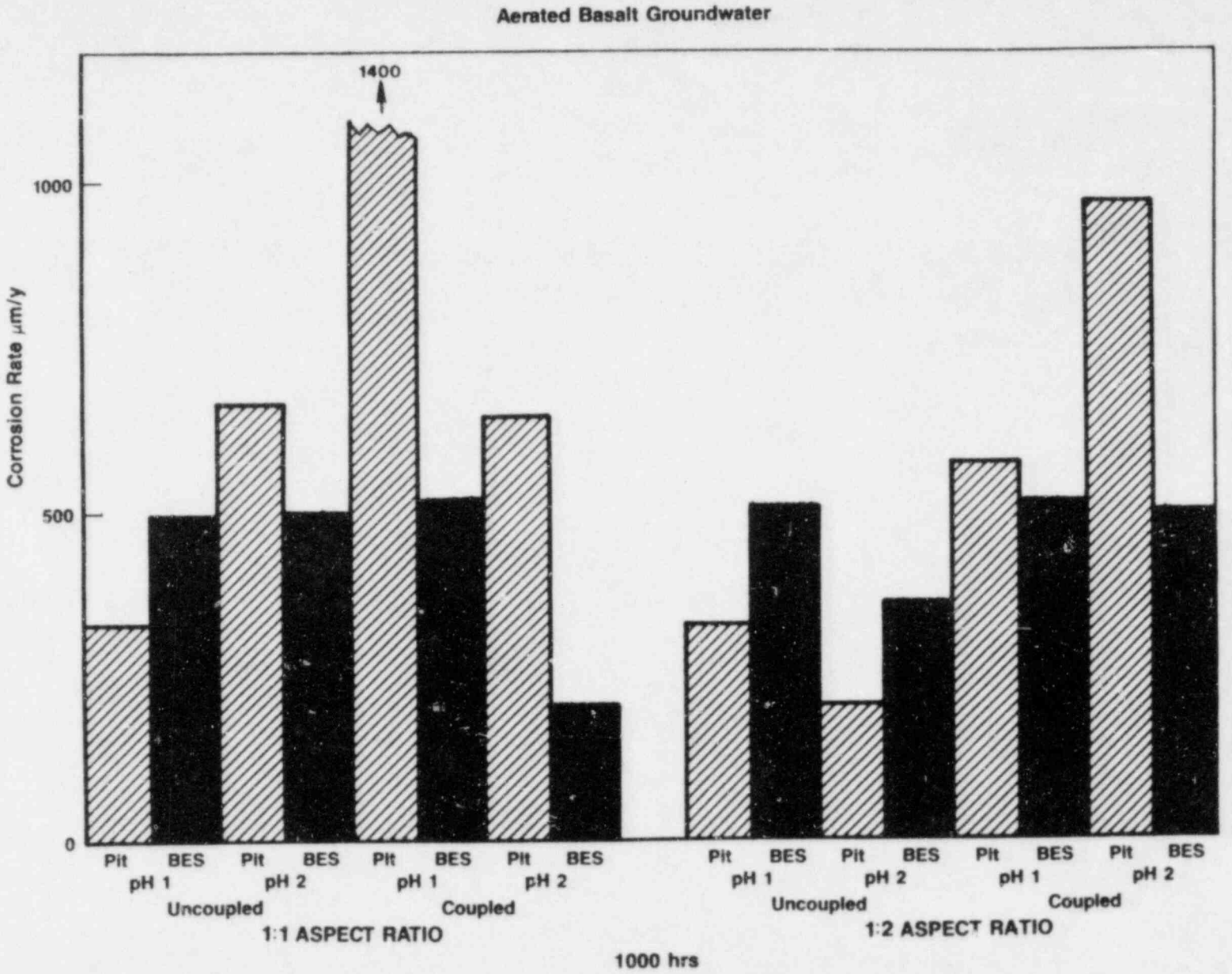

Figure 3.10. Results of 1000-hour weight-loss tests performed on simulated pits in aerated basalt groundwater at 90 C.

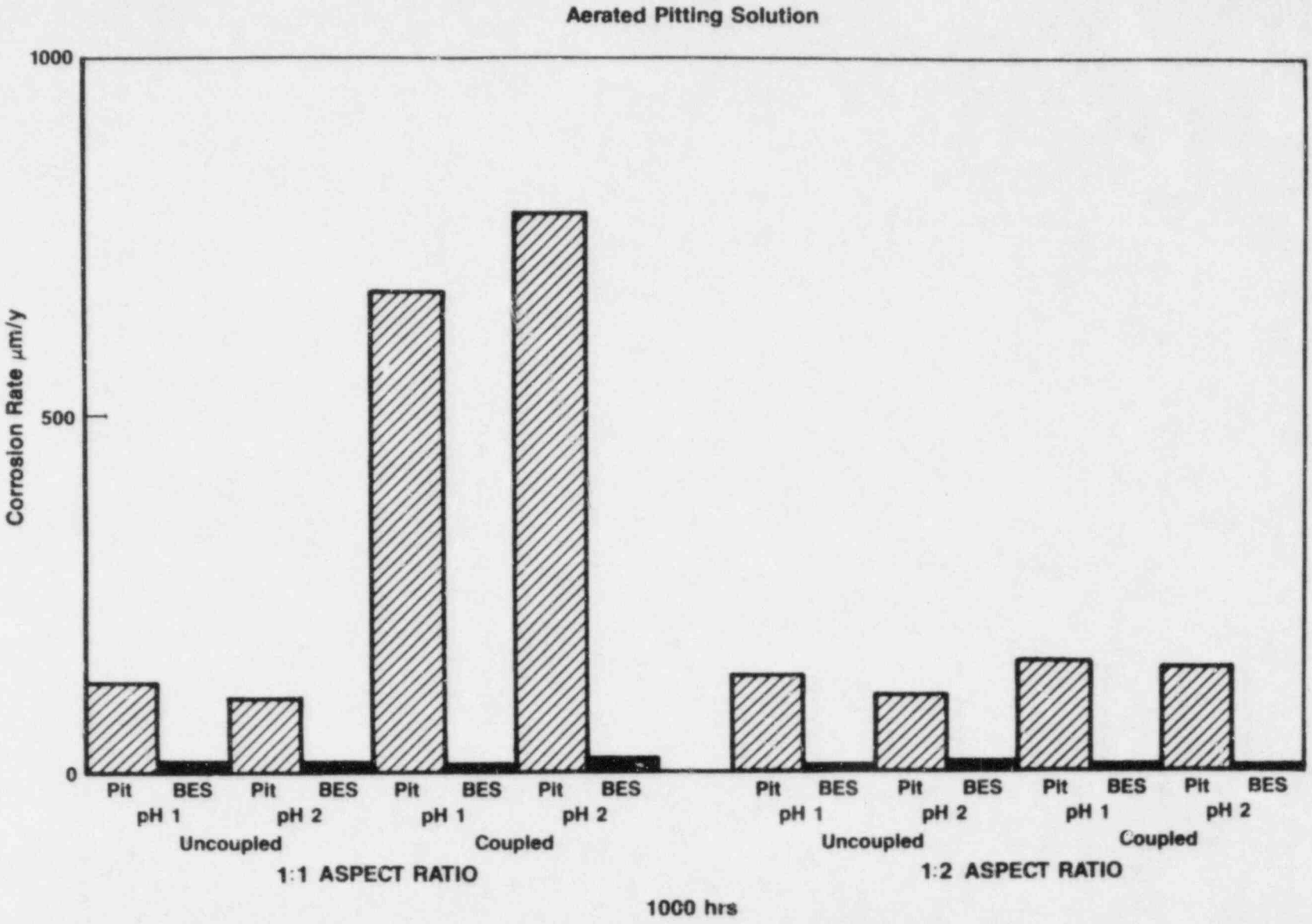

Figure 3.11. Results of 1000-hour weight-loss tests performed on simulated pits in an aerated pitting solution (Number 47 from potentiodynamic polarization studies) at 90 C.

effect of packing pH and the data for the pitting solution exhibited much less scatter than the data for the aerated basalt groundwater. Four diameter-to-depth ratios were studied (1:0.5, 1:1, 1:2, and 1:5) and all specimens were coupled.

Results of the 1000-hour exposure are given in Figure 3.12. As was observed in the previous tests, the corrosion rates of the BES specimens all were quite low. On the other hand, the corrosion rates of the pits increased with decreasing diameter-to-depth ratio, from 300 to 500 μm/yr at 1:0.5 to 1400 to 1700 μm/yr at 1:2. Below that diameter-to-depth ratio, the corrosion rate for the active-wall pit dropped off rapidly, from 1700 μm/yr at 1:2 to 250 μm/yr at 1:5, whereas the corrosion rate for the inactive-wall pit dropped off more gradually with increasing depth, from 1400 μm/yr at a diameter-to-depth ratio of 1:2 to 1050 μm/yr at a diameter-to-depth ratio of 1:5. The trend for the 1:2 and 1:5 diameter-to-depth ratio pits for the inert-wall case is comparable to that predicted from the inert-wall pit model, whereas the trend for the active-wall case is comparable to that estimated from the previous experiments. However, the trends in the data for the (shallow) pit of increasing pitting rate with increasing depth was not at all consistent with the results of the previous experiment (compare Figure 3.11 and 3.12), and suggest that the shallow pits were not fully occluded, resulting in passivation of the pit walls by the bulk electrolyte. Examination of the surfaces of the BES specimens with active walls confirmed this behavior; the surfaces inside the pits were passivated about one pit diameter down the pits. The reason why this phenomenon was not apparent in the previous weight-loss tests is not known, but may relate to the consistency of the packing paste or the rate of temperature increase of the cells during startup of the tests; the packing tends to expand upon heating and push out of the pits.

Because of the experimental difficulties encountered and the inherent scatter in the data, the weight-loss experiments with the active- and inert-wall pits are being repeated with duplicate specimens and lower diameter-to-depth ratios (1:10). The results of these experiments will be presented in the Annual Report for this program year.

3.3.3 Discussion

In spite of the experimental difficulties encountered, a clear trend is emerging from the pit-propagation studies. Simply stated, the inert- and the active-wall pits behave quite differently in the experimental studies. For the active-wall pits, corrosion rates drop quite rapidly with increased depth, and for relatively shallow pits, corrosion rates approach conditions of a fully occluded cell where the rate of attack is controlled by the reduction kinetics within the pit and not by a coupling effect with the boldly exposed surface. On the other hand, corrosion rates for the inert-wall pits fall much more gradually with increasing depth and follow the $1/\sqrt{h}$ relation predicted by the model for the inert-wall geometry developed earlier in the modeling studies.(3.3)

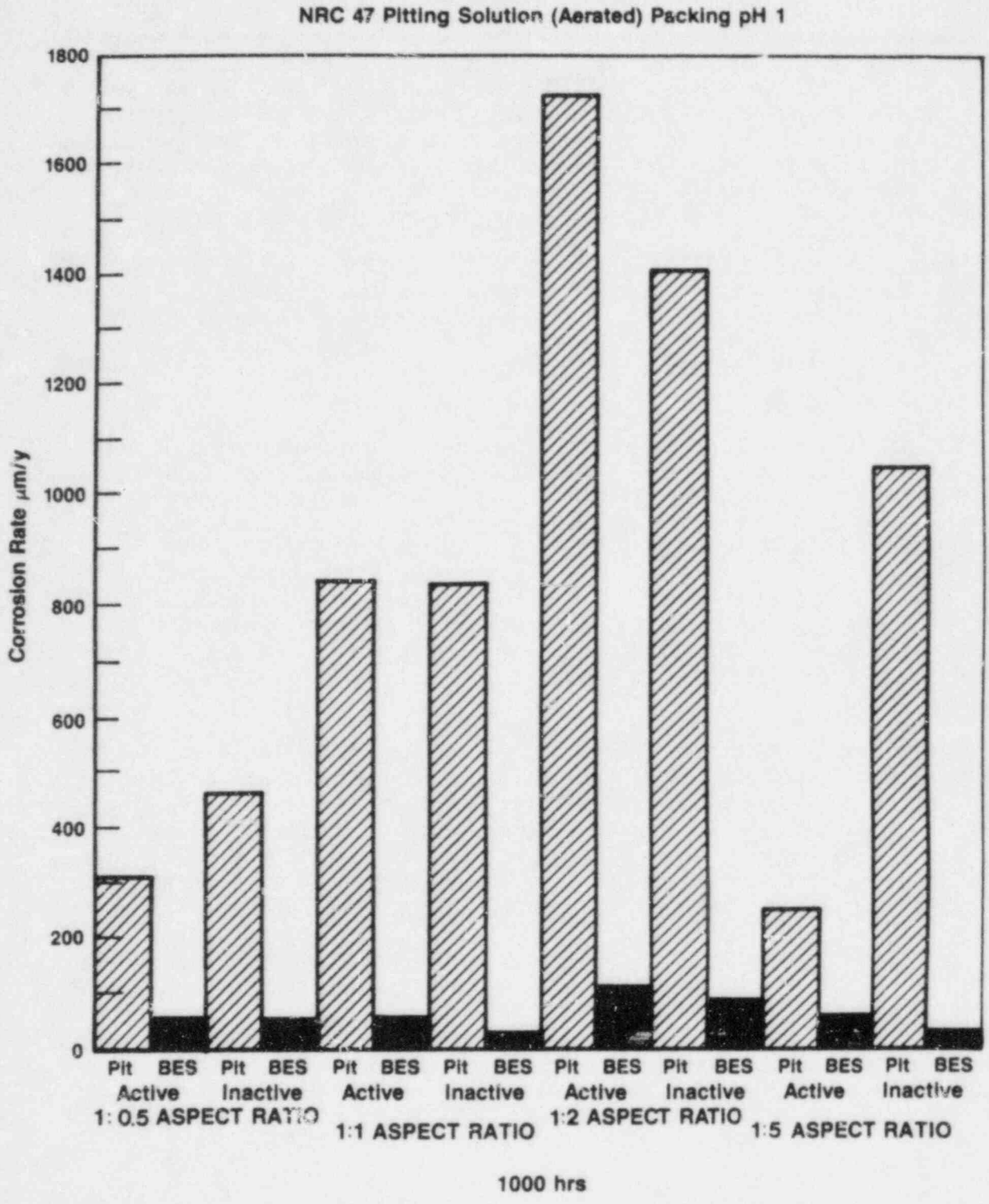

Figure 3.12. Effect of aspect ratio (depth to diameter) and pit wall activity on the corrosion rate of pit on BES specimens in 1000-hour weight-loss tests in an aerated pitting solution (Number 47 from the potentiodynamic polarization studies) at 90 C.

The results of the electrochemical studies shed considerable light on why the activity of the pit wall has such a large effect on the corrosion behavior. When the pit wall actively corrodes, high currents flow near the mouths of the pits, as shown schematically in Figure 3.13. This produces high potential drops near the pit mouth, effectively shielding the pit base from the potential field of the boldly exposed surface. This shielding effect does not occur for the inert-wall geometry, and thus high rates of corrosion occur for deeper pits.

These findings are quite consistent with the geometries of pits observed on carbon and low-alloy steels in natural environments. Deep, low diameter-to-depth ratio pits are rarely seen. Indeed, most pits are shallow with high diameter-to-depth ratios. For example, pits in natural gas pipeline may be as much as an inch in diameter and 0.25 inches deep.

The implication of these findings for the licensing effort for a carbon steel overpack is that pit-propagation models based on inert-wall geometries are inaccurate and highly conservative, and that more realistic pitting models can be developed which are nevertheless conservative but which estimate much thinner wall requirements for a 1000-year life.

These findings also have implications for other overpack materials and repositories. Thus, there is no apparent fundamental reason why the above approach is not applicable to a stainless steel overpack, which is proposed for the tuff repository.

An important issue is why lower diameter-to-depth ratio pits are observed more frequently in stainless steels than in carbon steel. The results of these studies suggest that this can occur as a result of high rates of reduction within the pits which drive the corrosion reaction. Thus, the fundamental difference between stainless steels and carbon steel, with regard to the pitting behavior, may lie in the nature of the hydrolysis reactions which occur within the pits and which produce protons that are subsequently reduced.

If this theory is correct, then rates of pit propagation for stainless steels can be estimated on the basis of electrochemical kinetics studies performed in simulated pitting environments.

3.4 JAERI-NRC Program Support

During this reporting period, carbon steel slow strain rate (SSR) specimens were prepared and forwarded to JAERI for use in their SSR experiments.

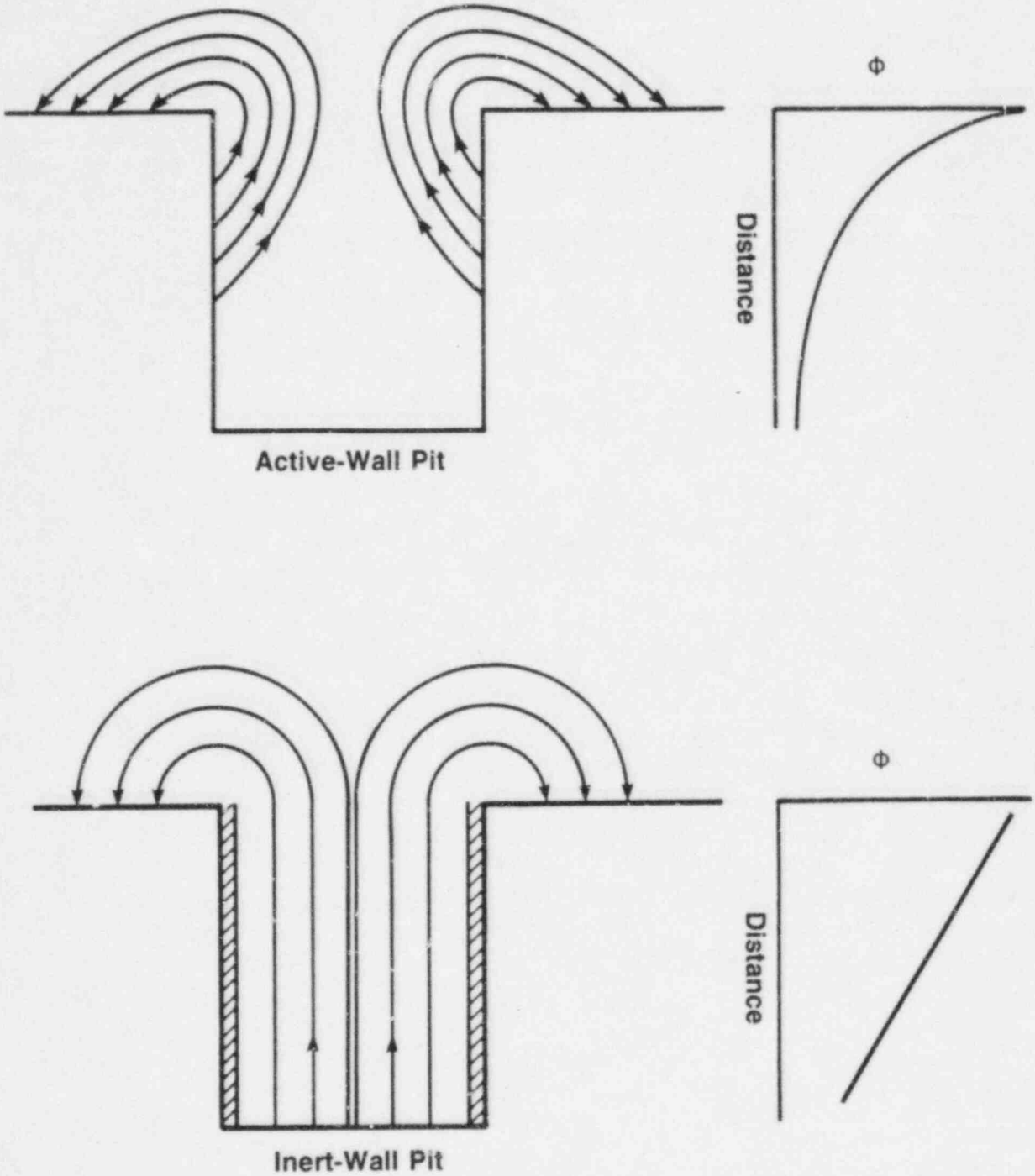

Figure 3.13. Schematic showing the postulated potential (ϕ) and current behavior for inert- and active-wall pits.

Direction of current flow is indicated by curved lines.

3.5 Future Work

3.5.1 Potentiodynamic Polarization Studies

The statistical analysis of the electrochemical data will be completed with the inclusion of the chemical analyses data. The final regression model will be developed. As discussed in the last quarterly report, H_2O_2 and perchlorate did not show an effect on the electrochemical parameters in the matrix of experiments. This behavior was attributed to the reduction of the concentration of these oxidizing ions in the solutions prior to performing the potentiodynamic polarization experiments. Several additional experiments were performed to investigate the transient behavior of these species. Based on this work, results of the electrochemical experiments with perchlorate will be analyzed and reported.

3.5.2 Pitting-Kinetics Studies

The weight-loss exposures on the simulated pit specimens will be completed and the data will be analyzed. Several electrochemical pit-propagation experiments will be performed. The objective of these experiments is to evaluate the effect of coupling on the potential (IR) profile down the pit.

3.5.3 Slow Strain Rate Studies

No SSR experiments are planned for next quarter. The SSR experiments on environments selected on the basis of the results of the potentiodynamic polarization studies will be resumed during the first quarter of the next program year.

3.5.4 JAERI-NRC Support Program

No activities are planned for next quarter on the JAERI-NRC support program. Activities on this task will be carried out as requested by JAERI and with the approval of NRC.

3.6 Corrosion Correlations

The objective of the corrosion-correlation effort is to provide information about corrosion processes that could affect overpack performance and to complement experimental work in this program. Studies in this effort are focused on general-corrosion modeling, pitting-corrosion modeling, and mechanical degradation.

3.6.1 General-Corrosion Modeling

Work is in progress to reformulate the general-corrosion model following the mathematical formalism described in the last quarterly report. Two aspects of the model that are being emphasized are improving the realism of the water-radiolysis description and generalizing the boundary

condition at the waste container. It is expected that the reformulation of the general-corrosion model and sample calculations using the new version will be completed during the remainder of the current program year.

3.6.2 Pitting-Corrosion Modeling

The pit-growth model originally developed under this program[3.3] was based on the familiar ionic-transport theory for a "binary electrolyte"[3.4], which consists of a solution containing one cation species and one anion species. The cation was taken to be the dissolving metal at the pit base and the anion was assumed to represent an "average" description of all the anion species that may be present. Ionic transport through the solution inside the pit was described using the mass-transport formalism for a dilute solution[3.5]. Important simplifying assumptions were that the pit was cylindrical in shape; the pit base consisted of bare metal which dissolved, causing pit growth; and the pit walls were chemically inert. These assumptions permitted a closed-form description of pit growth to be obtained.

More recently[3.6], this model was extended to include a more detailed analysis of cation dissolution at the pit base, which was described using Butler-Volmer kinetics. Both the dissolution (anodic) reaction and the backwards (cathodic) reaction were included. In addition, a number of important limiting cases were developed, based on solution-transport-limited kinetics and electrode-reaction-limited kinetics.

During this quarter, consideration was given to relaxing the assumption of chemically inert pit walls. This was undertaken in response to experimental studies of pitting being carried out under this program (Section 3.3 of this report) which indicate that chemical effects of the pit wall may be important.

To include the assumption of chemically active walls in a pit-growth model, care must be exercised since it is possible for the model to become prohibitively complex. With this in mind, we have developed a very elementary description of active-wall effects based on a correspondingly simple model of pit growth. Despite the simplicity of the model, however, some important effects are revealed with this approach.

For the present, the following assumptions are used:

(1) A two-dimensional, rectangular pit is considered, although the analysis could easily be applied to other configurations (e.g., a pit having circular cross section in a plane perpendicular to its length).

(2) The line parallel to the pit length midway between the two walls is assumed to be a line of symmetry.

(3) The length, h, of the pit is large compared to its width, d.

(4) Activity of the pit walls is described using linear-polarization behavior (a widely employed assumption in studies of electrochemical systems[3.7]) that is independent of spatial coordinates but which may vary quasistatically with time.

(5) No concentration gradients exist for any of the chemical species within the solution.

As a result of Assumption 5, the potential, ϕ, inside the pit satisfies the Laplace equation, i.e.,

$$D^2\phi=0 \tag{3-1}$$

However, because of Assumptions 1 to 3, one can show (e.g., Markworth and Kahn[3.8] and others) that Eq. 3-1 reduces, to lowest order, to the following expression:

$$\frac{d^2\phi(x)}{dx^2} = -\frac{2}{\sigma d}\, i(x) \tag{3-2}$$

where x is the distance measured along the pit length (taking x=0 at the pit opening), σ is the conductivity of the solution, and i is the current density crossing each of the two pit walls at position x (with $i>0$ for anodic currents and $i<0$ for cathodic currents). From Assumption 4, i(x) may vary only quasistatically with time, which means that Eq. 3-2 is valid at any given instant. Such time dependence results from pit growth and from chemical reactions taking place on the pit walls.

An important feature of Eq. 3-2 is that the potential, ϕ, is now a function only of x, its variation in this direction being of dominant importance because of Assumption 3. Thus, the major difference between Eq. 3-1 and 3-2 is that ϕ is a function of two spatial variables in Eq. 3-1, but a function of only one (x) in 3-2. However, the current crossing the active pit walls appears as an effective "source" term in Eq. 3-2.

We choose to express Assumption 4 mathematically as

$$i(x) = -\beta\,[\phi(x) - \phi_C] \tag{3-3}$$

where β and ϕ_C are parameters which describe the assumed linear relationship between ϕ and i. Clearly, the current i is cathodic (negative) for $\beta>0$ and $\phi<\phi_C$, but would become anodic for $\beta>0$ and $\phi>\phi_C$.

Combining Eq. 3-2 and 3-3,

$$\frac{d^2\phi}{dx^2} = \frac{2\beta}{\sigma d}\,(\phi - \phi_C) \tag{3-4}$$

Eq. 3-4 can be cast in dimensionless form by defining

$$\theta \equiv \phi \; / \; \phi_C \tag{3-5}$$

and

$$y \equiv x \left(\frac{2\beta}{\sigma d}\right)^{\frac{1}{2}} \tag{3-6}$$

from which we obtain

$$\frac{d^2\theta}{dy^2} = \theta - 1 \tag{3-7}$$

The general solution of Eq. 3-7 can be expressed in a number of different forms (e.g., Markworth and Kahn[3.9]). For the present, we express this solution as

$$\theta = 1 + Ae^{y} + Be^{-y} \tag{3-8}$$

where

$$A \equiv \theta_o - 1 - \tfrac{1}{2}\left[e^{y_h}(\theta_o - 1) - \theta_h + 1\right] \operatorname{csch} y_h \tag{3-9}$$

$$B \equiv \tfrac{1}{2}\left[e^{y_h}(\theta_o - 1) - \theta_h + 1\right] \operatorname{csch} y_h \tag{3-10}$$

with

$$\theta_o \equiv \phi_o \; / \; \phi_C \tag{3-11}$$

$$\theta_h \equiv \phi_h \; / \; \phi_C \tag{3-12}$$

$$y_h \equiv h \left(\frac{2\beta}{\sigma d}\right)^{\frac{1}{2}} \tag{3-13}$$

where ϕ_o and ϕ_h are the values of the potential at the pit opening ($x=0$) and pit base ($x=h$), respectively. Actually, the potential ϕ_h is, in general, related to the current density crossing the pit base, i.e.,

$$-\sigma \frac{d\phi}{dx} \; (x = h)$$

through some electrode-kinetics expression (e.g., Butler-Volmer kinetics[3.6]); however, this relationship is not considered here.

The important conclusion to be drawn from this model is the fact that the potential (as represented by θ in Eq. 3-9) varies with position along the pit length in a decidedly nonlinear manner. This can be contrasted with corresponding behavior for the case of inert walls, for which the potential does vary linearly with position along the crevice length[3.3]. The precise manner in which θ varies with y (i.e.,

in which ϕ varies with x) depends upon the specific numerical values selected for the various parameters, ϕ_o, ϕ_h, ϕ_c, β, σ, h, and d. Some specific cases have been treated elsewhere, by Fessler et al.[3.10], for simulated crevice configurations having very large length-to-thickness ratios. It was found here, for example, that the largest potential gradients within the crevices existed near the crevice opening. This latter behavior was observed in some pitting experiments conducted at Battelle, although the overall kinetics was not likely the same for the two cases.

3.6.3 Mechanical-Degradation Analysis

Issues relating to the mechanical aspects of stress-corrosion cracking are currently being addressed. The aim of this study is to develop a worst-case scenario based on a combination of the most aggressive cracking agent and the loading conditions that lead to such cracking.

Several species have been identified as potential agents for inducing stress-corrosion cracking in mild-steel container material. These species include carbonates/bicarbonates, nitrates, hydroxides, and ferric chloride or chloride plus ferric oxide or hydroxide[3.11]. Although some of these species are not present in any significant quantities in basalt groundwater, it is possible that they could concentrate in the vicinity of the container. Contamination of the groundwater with fertilizers could, for example, be a source of nitrates. Chlorides are present in the groundwater, and the corrosion of the container material will produce ferrous ions that may be oxidized to ferric ions by radiolysis or oxygen ingress in the repository[3.11, 3.12].

It should be noted that species produced in radiolysis of groundwater could alter the stress-corrosion cracking behavior of the container material significantly by altering the local pH and electrochemical potential. For the present, however, effects of radiolysis are not considered.

Research conducted on line-pipe steels in carbonate/bicarbonate environment has shown that the material undergoes stress-corrosion cracking when loaded to between 40 and 100 percent of the yield strength of the steel[3.13]. This threshold stress is influenced by factors such as the concentration of the chemical environment, electrochemical potential, and composition and processing of the steel[3.13]. Along similar lines, cracking in nitrate and hydroxide environments requires stresses that exceed the yield stress of the material[3.14]. Work by Ondrejcin et al.[3.15], pertaining to radioactive waste storage tanks, has shown that nitrite and hydroxide ions act as inhibitors in complex waste composition. Although the complex waste composition is not directly related to the container-service performance, nitrate and hydroxide ions constitute the common link between the two environments. It was

determined that nitrate concentration in the storage tanks should not exceed 5.5 M* and that a minimum combined nitrite and hydroxide concentration of 1.2 M should be maintained in the waste composition[3.15]. These concentration limits are valid for temperatures up to 70 C and were developed for ASTM A285-B and ASTM A516-70 material[3.15]. For ASTM A285-B and A212-B material, it was noted that a 50-percent sodium nitrate environment produced the most severe cracking at 90 to 95 C[3.16].

Studies pertaining to the waste storage tanks[3.15, 3.16] indicated that cracking of the tanks was related to residual stresses in the material. As-welded plates of carbon steel cracked readily in a 50-percent sodium nitrate environment, while stress-relieved samples were immune to stress corrosion cracking[3.16]. The stress-relieving operation involved placing the specimen in a furnace maintained at less than 316 C; heating to 593 C at a rate of less than 200 C/hr; maintaining the furnace at 593 C for 30 minutes; then cooling to 316 C at a rate of less than 260 C/hr. The data in this study seem to suggest that stress-relieved specimens did not crack when stressed up to 150 percent of the yield stress of the material. Work by Conor[3.17], on the other hand, suggests that cracking in annealed mild steel will occur when the applied stress reaches the yield stress of the material. This work was undertaken on a 0.1-percent carbon steel in 4N** ammonium nitrate[3.17].

One of the major differences in the studies performed by Conor[3.17] and Costas[3.16] is that Conor conducted slow-strain-rate tests while Costas conducted constant-displacement experiments to study stress-corrosion cracking susceptibility. The slow-strain-rate test is more severe in that the specimen experiences continually increasing strain--fresh material is exposed to the environment as the material is strained. In a constant-displacement test, as cracking occurs the stress is relieved, thereby reducing the severity of the test condition. This suggests that the mechanical loading conditions also play a role in determining a threshold stress for stress-corrosion cracking. If the loads fluctuate, such load-cycling will lower the threshold for stress-corrosion cracking.

Finally, the stress-corrosion studies conducted in ferric chloride environment indicate that carbon steel cracks readily in this environment at chloride concentrations that are typical of basalt groundwater[3.12]. Cracking appears to be most severe in the temperature range of 150 to 250 C[3.12]. The study has not defined the stresses at which cracks initiate.

---

* Molar.
** Normal.

Mechanical issues related to stress-corrosion cracking have been discussed in a very general sense. Few quantitative data exist in the literature relating stress to other parameters such as temperature, pH, potential, and concentration of various ionic species. It is obvious that all the permutations and combinations would produce a matrix requiring a large number of experiments. The material parameters, such as composition of the material and the method of heat treatment, are other variables that have not been addressed in this study. In addition, as noted earlier, cyclic stresses will play an important role in determining stress-corrosion susceptibility.

While it may be argued that the container will be subjected to compressive stresses during service and that stress-corrosion cracking does not occur under such conditions, a recent study of an aluminum alloy has shown that stress-corrosion cracking can occur under compressive loading(3.18). This is another issue that needs to be addressed and may become an important topic for study in this task.

3.7 References for Section 3

(3.1) "Long-Term Performance of Materials Used for High-Level Waste Packaging", D. Stahl and N. E. Miller (Compilers), NUREG/CR-3900, Vol 4, BMI-2127 (July, 1985), pp 3-2 ff.

(3.2) "Long-Term Performance of Materials Used for High-Level Waste Packaging", D. Stahl and N. E. Miller (Compilers), NUREG/CR-3900, Vol 4, BMI-2127 (July, 1985), pp 3-14 ff.

(3.3) "Long-Term Performance of Materials Used for High-Level Waste Packaging", D. Stahl and N. E. Miller (Compilers), NUREG/CR-3427, Vol 4, BMI-2113 (June, 1984), pp 3-126 ff.

(3.4) J. S. Newman, Electrochemical Systems, Prentice-Hall, Inc. (Englewood Cliffs, N.J., 1973), pp 223 ff and elsewhere within volume.

(3.5) J. S. Newman, op. cit., pp 217 ff.

(3.6) "Long-Term Performance of Materials Used for High-Level Waste Packaging", D. Stahl and N. E. Miller (Compilers), NUREG/CR-4379, Vol 2, (September, 1985), pp 3-29 ff.

(3.7) W. H. Smyrl, "Current and Potential Distributions in Corrosion Systems", in Tutorial Lectures in Electrochemical Engineering and Technology, R. Alkire and T. Beck, eds., AIChE Symp. Series, No. 204, Vol 77, Am. Inst. Chem. Engrs. (New York, 1981), p 152.

(3.8) A. J. Markworth and L. R. Kahn, "A Hierarchical Model for Mass Transport Kinetics Within a Crevice-Like Region", in Predictive Capabilities in Environmentally Assisted Cracking, R. Rungta, ed., PVP-Vol. 99, Am. Soc. Mech. Engrs. (New York, 1985), p 143.

(3.9) A. J. Markworth and L. R. Kahn, "Mathematical Modeling of Electrochemical Conditions Within a Stress Corrosion Crack", Final Report from Battelle's Columbus Division to Electric Power Research Institute on Research Project RP2258-2 (in preparation).

(3.10) R. R. Fessler, A. J. Markworth, and R. N. Parkins, "Cathodic Protection Levels Under Disbonded Coatings", Corrosion-NACE, 39 (1983) 20.

(3.11) J. A. Beavers, N. G. Thompson, and R. N. Parkins, "Stress Corrosion Cracking of Low-Strength Steels in Candidate High Level Waste Repository Environments", Topical Report, NUREG/CR-3861, (1984).

(3.12) "Long-Term Performance of Materials Used for High-Level Waste Packaging", D. Stahl and N. E. Miller (Compilers), NUREG/CR-3900, Vol. 4, Annual Report (June, 1985), pp 3-42.

(3.13) R. R. Fessler, "Preventive Measures for Pipeline Stress-Corrosion Cracking Described", Oil & Gas Journal (January, 1980), pp 80-90.

(3.14) W. Frank and L. Graf, "Mechanism of Intergranular Corrosion and Intergranular Stress-Corrosion Cracking in Mild Steels", Res. Mechanica, 13 (1985), pp 251-264.

(3.15) R. S. Ondrejein, S. P. Rideout, and J. A. Donovan, "Control of Stress-Corrosion Cracking in Storage Tanks Containing Radioactive Waste", Nuclear Technology, 44 (1979), pp 297-306.

(3.16) L. P. Costas, M. L. Holzworth, and W. C. Rion, "Stress Corrosion Cracking of Carbon Steel in Simulated Waste Solution", DP-1023, Savannah River Laboratory, E.I. DuPont De Nemours & Co., Aiken, South Carolina (1966).

(3.17) P. C. Conor, "Stress-Corrosion Cracking Thresholds in Normalized Mild Steel", Metals Australasia (June-July, 1984), pp 8-9.

(3.18) W. Y. Chu, C. M. Hsiao, and J. W. Wang, "Stress Corrosion Cracking of an Aluminum Alloy Under Compressive Stress", Metallurgical Transactions, Vol. 16A (1985), pp 1663-1670.

4. INTEGRATED SYSTEM PERFORMANCE

The integrated system performance task is designed to provide a better understanding of phenomena that would impact the long-term performance of waste packages at the repository system level. These studies will provide insight on possible chemical conditions of the waste package environment, effects of cladding failure on radionuclide releases, and combined-effects processes. Knowledge gained in these studies will aid in assessing system performance models for nuclear waste packages. During this quarter, continued emphasis has been placed on water-chemistry studies, groundwater-radiolysis studies, and integral experiments.

Water-chemistry studies will provide information on how groundwater chemistry and the corrosion of metallic barriers affects the waste form, as well as how waste-form dissolution alters the local water chemistry. These studies will also provide information on the chemical speciation of radionuclides released from the waste form for assessing the transport rate of the radionuclides through the waste package.

The groundwater-radiolysis studies will provide information on the concentrations of radiolytic species in the vicinity of waste packages. These species have the potential to affect the corrosion of the metallic barriers, the rate of waste-form dissolution, and the chemical speciation of the radionuclides released from the waste form. Radiolysis of groundwater in the waste package environment can thus affect the containment time for a waste package as well as the release rates of radionuclides from the waste package to the underground facility.

The integral experiments are being performed to provide information on the effects of cladding degradation on radionuclide release rates, performance of spent-fuel waste forms in various environments, groundwater radiolysis, and combined-effects processes. To accomplish these objectives, the integral experiments have been designed to simulate characteristics of repository environments for spent-fuel materials in deep-mined repositories in tuff, basalt, and granite media.

4.1 Water Chemistry

Work is in progress to enlarge the set of chemical species treated by the water-chemistry model so that it will be applicable to the dissolution of spent fuel. This requires the collection and evaluation of thermodynamic data for aqueous uranium species and uranium complexes, and the incorporation of these species into the water chemistry code. It is expected that extension and testing of the revised code will be completed during the next quarter.

4.2 Groundwater Radiolysis Studies

Radiolysis of groundwater in the vicinity of waste packages can cause changes in water chemistry which may influence processes such as

corrosion and radionuclide transport. Such effects can in turn impact the long-term performance of the affected waste packages. Perturbations to the local water chemistry can include changes in pH and oxygen potential, as well as the production of additional species which may have a deleterious effect on the performance of waste package materials. As reported previously, other investigators have observed that gamma radiation may have adverse effects on the time-to-failure performance measure for metal components which are exposed to water[4.1, 4.2, 4.3].

An objective of these studies is to develop a generalized model for analyzing the radiolysis of groundwater systems and the radiolysis of groundwater systems whose composition has been altered by the presence of other materials such as packing and corrosion products. This model will provide information on the expected concentrations of radiolysis products in the vicinity of the metallic components of waste packages. Such information will support the overpack corrosion studies in guiding the selection of experimental conditions for materials performance tests. The model will also provide a means of assessing other radiolysis models such as those required in the general-corrosion model, described in Section 3.6. The model will provide a vehicle for determining effective rate constants for complex reactions which may be incorporated in the water radiolysis-component of the general-corrosion model.

The approach used in these studies is to first develop a description for the radiolysis of pure water which might contain hydrogen and/or oxygen. This description is being extended to account for the presence of anions and cations which may be present in significant concentrations in groundwaters of interest. As the description of groundwater radiolysis is developed, it is being benchmarked against experimental data available in the literature. As part of this effort, gamma-energy deposition calculations were performed to determine energy deposition rates to groundwater and materials surrounding spent fuel and commercial high-level waste packages. Results of these energy deposition calculations have been reported previously[4.4]. In earlier studies[4.4], several mechanisms for the radiolysis of water were evaluated on the bases of their ability to predict the data from water-radiolysis experiments reported in the literature. Of these, the mechanism of Rosinger and Dixon[4.5] was chosen as a basis mechanism upon which a generalized description for groundwater radiolysis would be developed. Work this quarter has been directed towards extending this description to account for the presence of bicarbonate anions in groundwaters. Bicarbonate anions are a significant species in tuff groundwaters having a reported concentration of 120 mg/liter[4.6], and are present in basalt groundwaters at concentrations on the order of 1.8 meq/liter[4.7]. A bicarbonate anion concentration of 23 mg/liter has also been reported for Permian Basin brine[4.8].

4.2.1 Radiolysis of Groundwaters Containing Bicarbonate Anions

To develop a mechanism for the radiolysis of groundwaters containing bicarbonates, it was necessary to consider the interactions of CO_2 with

Table 4.1. Reactions added to the groundwater which account for interactions between radiolytic species and bicarbonate species.

No.	Reaction
1.	$O_2^- + HCO_3^- \rightarrow HO_2^- + CO_3^-$
2.	$O_2^- + CO_3^- \rightarrow O_2 + CO_3^{2-}$
3.	$HCO_3^- \rightarrow CO_2 + OH^-$
4.	$CO_2 + OH^- \rightarrow HCO_3^-$
5.	$OH + HCO_3^- \rightarrow CO_3^- + H_2O$
6.	$H + HCO_3^- \rightarrow H_2 + CO_3^-$
7.	$e^- + HCO_3^- \rightarrow H + CO_3^{2-}$
8.	$OH + CO_3^{2-} \rightarrow OH^- + CO_3^-$
9.	$HCO_3^- + OH^- \rightarrow CO_3^{2-} + H_2O$
10.	$CO_3^- + CO_3^- \rightarrow CO_2 + CO_2 + HO_2^- + OH^- - H_2O$
11.	$H^+ + HCO_3^- \rightarrow H_2CO_3$
12.	$H_2CO_3 \rightarrow H^+ + HCO_3^-$
13.	$CO_2 \rightarrow H_2CO_3 - H_2O$
14.	$H_2CO_3 \rightarrow CO_2 + H_2O$
15.	$H_2CO_3 + OH^- \rightarrow HCO_3^- + H_2O$
16.	$OH + CO_2 \rightarrow HCO_3$
17.	$HCO_3^- + H^+ \rightarrow CO_2 + H_2O$
18.	$CO_2 + H_2O \rightarrow HCO_3^- + H^+$

Table 4.2. Rate constants for the reactions shown in Table 4.1.

Reaction Number	Rate Constant		Reference Number
1	1.5×10^{6}	liter/mole·sec	4.16
2	1.5×10^{7}	liter/mole·sec	estimated (see text)
3	1×10^{-4}	sec^{-1}	4.10
4	1.4×10^{4}	liter/mole·sec	4.10
5	5.5×10^{7}	liter/mole·sec	4.14
6	2×10^{4}	liter/mole·sec	4.15
7	6×10^{5}	sec^{-1}	4.17
8	4.2×10^{8}	liter/mole·sec	4.11
9	6×10^{9}	liter/mole·sec	4.10
10	6.25×10^{6}	liter/mole·sec	4.11 (see text)
11	4.7×10^{10}	liter/mole·sec	4.10
12	8×10^{6}	sec^{-1}	4.10
13	4.3×10^{-2}	sec^{-1}	4.12, 4.10
14	1.5×10^{1}	sec^{-1}	4.10
15	6×10^{9}	liter/mole·sec	estimated (see text)
16	1×10^{5}	liter/mole·sec	estimated (see text)
17	5.6×10^{4}	liter/mole·sec	4.10
18	4.3×10^{-2}	liter/mole·sec	4.10

radiolysis products. This requirement follows in part from the equilibrium between CO_2 and H_2CO_3[4.9, 4.10].

The mechanism developed this quarter is shown in Tables 4.1 and 4.2. The elementary reactions are shown in Table 4.1 and the rate constants and literature sources are shown in Table 4.2. Data were available for most of these reactions.

Reactions 1, 5 through 7, 9, 11, and 17 account for direct reactions of the bicarbonate anion with radiolytic species. Reaction 3 accounts for the direct decomposition of the bicarbonate anion. Reactions 4, 15, and 18 are direct sources of bicarbonate anions. In addition to these reactions which represent the direct sources and sinks of bicarbonate anions, several other reactions are needed in the model to account for interactions with species produced through the bicarbonate-anion reactions. These other species are CO_2, CO_3^{2-}, CO_3^{-}, HCO_3^{-}, and H_2CO_3. Carbon dioxide is produced in Reactions 3, 10, 14, and 17 and it is consumed in Reactions 4, 13, 16, and 18. Carbonic acid is produced in Reactions 11 and 13, and is consumed in Reactions 12, 14, and 15. The presence of dissolved carbon dioxide and carbonic acid tend to contribute to acid conditions. This is countered by the presence of hydroxide ions which react with carbon dioxide to form bicarbonate, and with bicarbonate to form carbonate anions. This can also be countered through the hydrolysis of bicarbonate which would produce hydroxide ions. Hydrolysis of bicarbonate is not presently included in the groundwater-radiolysis model.

Rate constants and literature sources for these reactions are shown in Table 4.2. Rate constants are available for all of the reactions except 2, 6, 10, 15, and 16. Rate constants for these reactions were estimated based on comparison with other reactions and data in the literature.

Keene, et al.[4.13] have determined the rate constant for Reaction 16 to be less than 10^6 liters/mole·sec. In the groundwater-radiolysis model, this rate constant is provisionally set to 10^5 liters/mole·sec. The model is not believed to be sensitive to this rate constant since the magnitude of the rate constant is low and the concentration of one of the reactants, OH, is also generally low.

The rate constant for Reaction 15 is stated to be essentially instantaneous by Cotton and Wilkinson[4.9]. For the purpose of estimating a rate constant, Reaction 15 was assumed to be analagous to Reaction 9. The rate constant for Reaction 15 was therefore estimated to be 6×10^9 liters/mole·sec, the same as for Reaction 9. The value of 6×10^9 liters/mole·sec is also in the diffusion-limited regime, making it consistant with the statement of Cotton and Wilkinson[4.9] that it is instantaneous.

Weeks and Rabani[4.11] have observed evidence for the bimolecular removal of the carbonate anion such as shown in Reaction 10. They proposed the following reactions:

$$CO_3^- + CO_3^- = CO_2 + CO_4^{2-}$$

or

$$CO_3^- + CO_3^- = 2CO_2 + HO_2^- + OH^- - H_2O.$$

The second reaction was chosen to be included in the model because all of the product species could be accounted for with the existing reaction set. Inclusion of the first reaction would have included a species (CO_4^{2-}) with a source and no sink and thus would have been unrealistic. Weeks and Rabani[4.11] have twice measured this rate constant to be 7.25×10^7 liters/mole·sec. A value of 6.25×10^6 liters/mole·sec is therefore used in the model.

For the reaction between H atoms and bicarbonate (Reaction 6), Nehari and Rabani[4.15], give the ratio of the rate constant for H^+ bicarbonate to the rate constant for $H + O_2$ to be 1.0×10^{-6} liters/mole·sec. Using a value of 2.0×10^{10} liters/mole·sec for the latter rate constant (taken from the groundwater-radiolysis model), the value of the H^+ bicarbonate rate constant was calculated to be 2×10^{-4} liters/mole·sec.

Experiments performed by Schmidt[4.16] imply that for Reactions 1 and 2 the first is rate-controlling. Thus, the rate of Reaction 2 must be much greater than the rate of Reaction 1. The rate constant for Reaction 2 was therefore taken to be ten times that of Reaction 1.

4.2.2 Simulation of Groundwater Radiolysis

The groundwater-radiolysis model was used in four simulations. The water composition for each simulation is shown in Table 4.3. Each simulation used identical initial concentrations of H^+, OH^-, H_2, and O_2. The composition of each did vary, however, with respect to the presence of Cl^-, Fe^{2+}, and HCO_3^- species. When present, these species had identical initial concentrations, as is shown in Table 4.3. The H^+ and OH^- concentrations are based on an assumption of an initial pH of 9. This is consistent with values reported in the literature[4.18]. The concentrations of Cl^- and HCO_3^- are derived from concentrations reported in the literature[4.7]. The initial concentration of H_2 is taken as a typical background concentration and its estimation is described in Ref. 4.9. The concentration of O_2 is based on an assumed concentration of 1 ppb, and the initial concentration of Fe^{2+} is based on an assumed initial concentration of .04 mg/liter as has been reported for tuff groundwater[4.6]. This is also consistent with a ferrous concentration of .03 mg/liter reported for Grande Ronde basalt groundwater[4.18]. The dose rate used in each simulation was a constant 1.0×10^{14} eV/liter·sec.

Figure 4.1 shows the value of pH calculated at 3×10^4 seconds into each of the four simulations. As can be seen, the pH decreases to values below 3 in each case where bicarbonate was present and remains alkaline where bicarbonate was not present. This large shift to acidity may be a shortcoming of the present version of the model, which does not yet

Table 4.3. Initial species concentrations for groundwaters used in radiolysis simulations.

Simulation	Initial Concentration (moles/liter)						
	H^+	OH^-	H_2	O_2	Cl^-	Fe^{2+}	HCO_3^-
A	1×10^{-9}	1×10^{-5}	4×10^{-10}	5.6×10^{-8}	0	1.0×10^{-6}	1.8×10^{-3}
B	1×10^{-9}	1×10^{-5}	4×10^{-10}	5.6×10^{-8}	8.75×10^{-3}	0	1.8×10^{-3}
C	1×10^{-9}	1×10^{-5}	4×10^{-10}	5.6×10^{-8}	8.75×10^{-3}	1.0×10^{-6}	0
D	1×10^{-9}	1×10^{-5}	4×10^{-10}	5.6×10^{-8}	0	1.0×10^{-6}	0

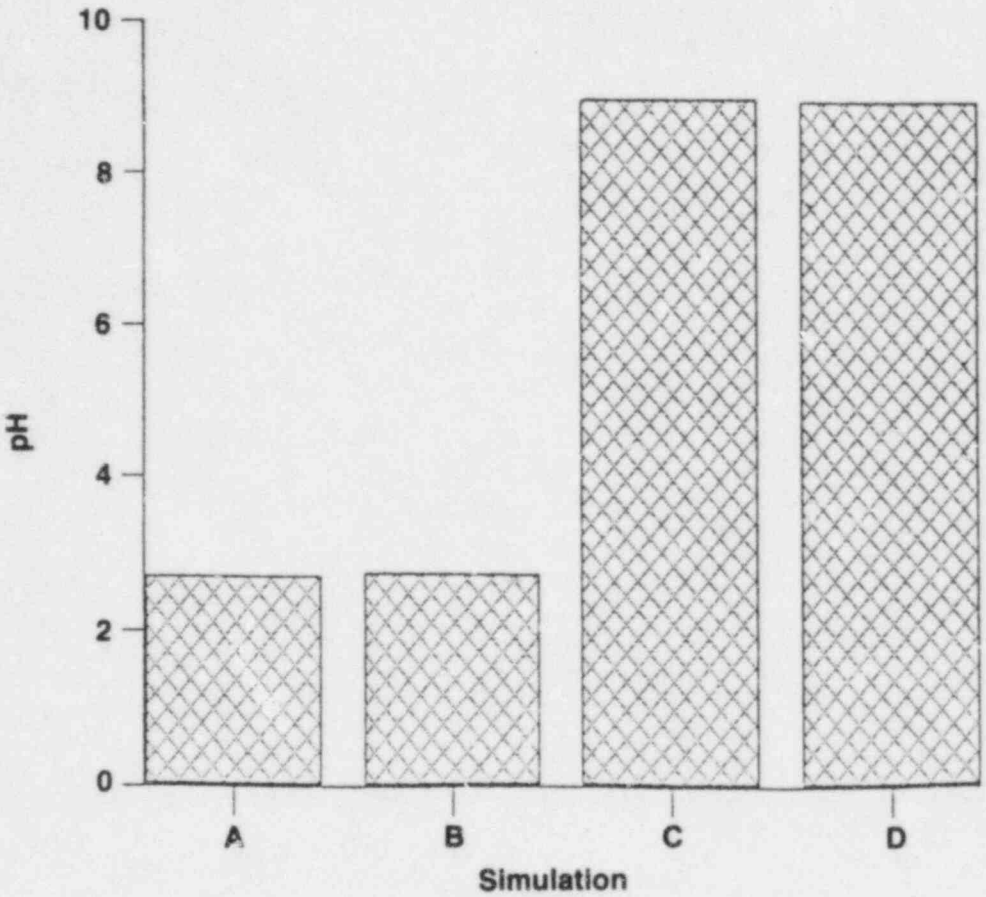

Figure 4.1. Calculated values of pH for each of the four simulations at 3×10^4 seconds.

As described in the text, acidic values of pH for Cases A and B may be a result of a shortcoming of the present version of the model.

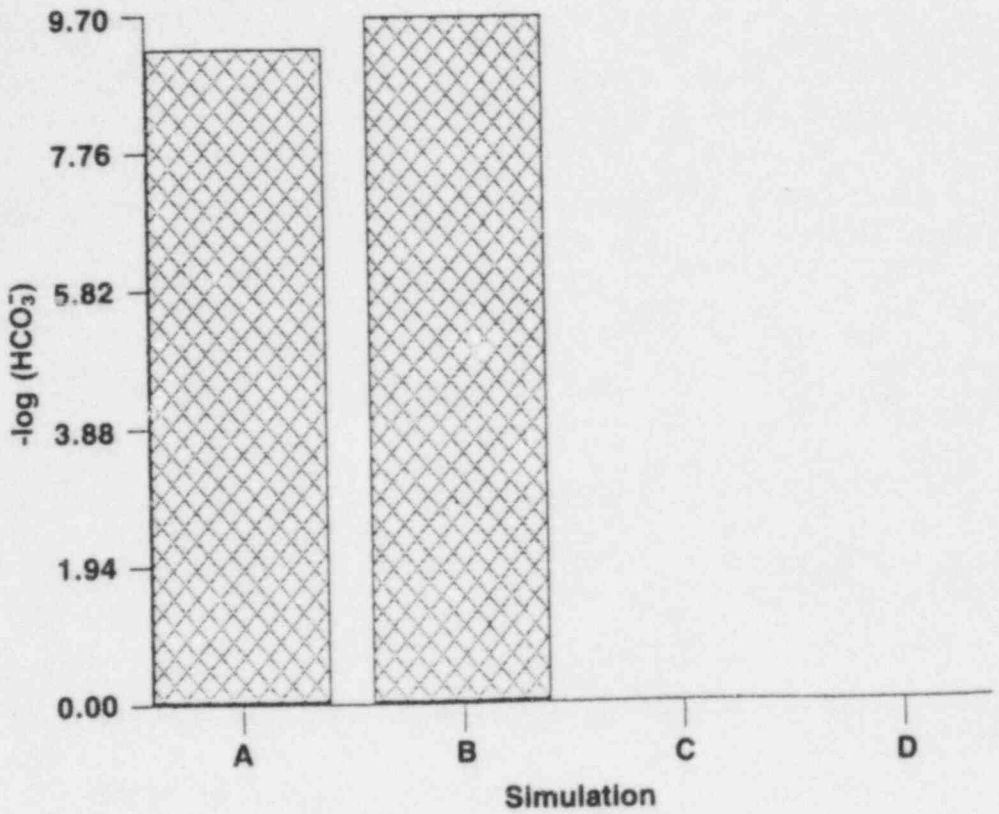

Figure 4.2. Concentrations of bicarbonate anion at 3×10^4 seconds for Cases A and B.

account for the hydrolysis of bicarbonate anion. Hydrolysis of this anion would produce additional hydroxide ions by the reaction

$$HCO_3^- + HOH \rightarrow H_2CO_3 + OH^-$$

Figure 4.2 shows that for simulation Cases A and B, which included bicarbonate, most of the bicarbonate was converted to other species.

Figure 4.3 shows the dissolved-oxygen concentration calculated for each of the four simulations at 3×10^4 seconds. Most of the initial dissolved oxygen (5.6×10^{-8} mole/L) was consumed for Cases A and D. The presence of ferrous ions in each of these cases is likely to be indirectly responsible for the reduction in oxygen concentration. The reduction in oxygen concentration was not quite as effective for Case C (2.13×10^{-9} mole/L) which also contained ferrous ions. Here the presence of chloride species apparently interfered with the ability of the ferrous ions to control the dissolved oxygen concentration. In Case C, the initial chloride concentration was much higher (8.75×10^{-3} mole/L) than the initial ferrous concentration (1.0×10^{-6} mole/L). This is a significant result and requires further investigation. It is important to determine whether chloride species can interfere with the ability of ferrous species to reduce the oxygen concentration in a radiation environment or if this behavior is a result of the current mechanism in the model.

Figure 4.4 shows the H_2O_2 concentration calculated at 3×10^4 seconds for each of the simulations. Here the calculated concentrations are seen to fluctuate between 1.73×10^{-9} and 7.65×10^{-7} mole/liter. Adding hydrolysis of bicarbonate to the model may affect calculated values of H_2O_2 for Cases A and B.

Figure 4.5 shows that the dissolved-hydrogen concentration was relatively insensitive to the changes in water chemistry for the four simulations.

These calculations indicate that the bicarbonate module of reactions requires improvement. It is believed that the addition of reactions describing the hydrolysis of bicarbonate will provide improved behavior with respect to calculated pH.

4.3 Integral Experiments

The integral experiments provide a means of examining interactions that may occur between components of the waste package and repository in various relationships. In particular, the integral experiments bring together elements of repository environments with metallic and nonmetallic components of the waste package and waste form. This approach allows for observing synergisms which may occur as greater degrees of freedom are introduced into the system. Influences of packing material, corrosion products, and radiation on groundwater chemistry may induce different performance characteristics from waste-package components than might

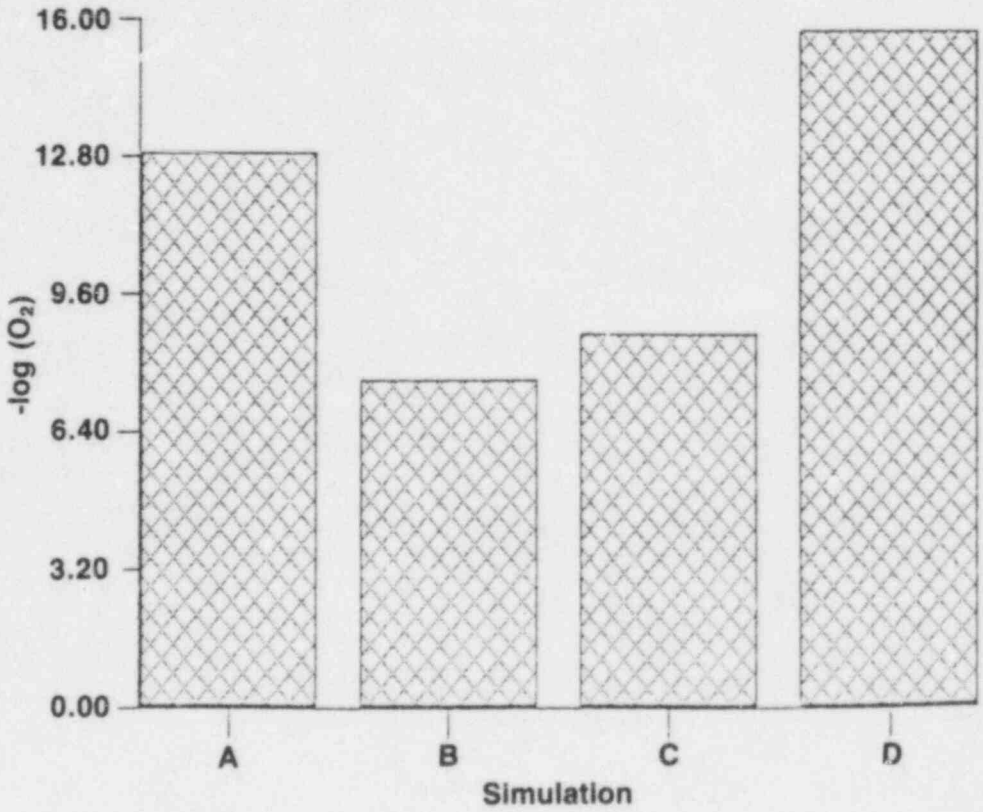

Figure 4.3. Concentration of dissolved oxygen calculated at 3×10^4 seconds for each simulation.

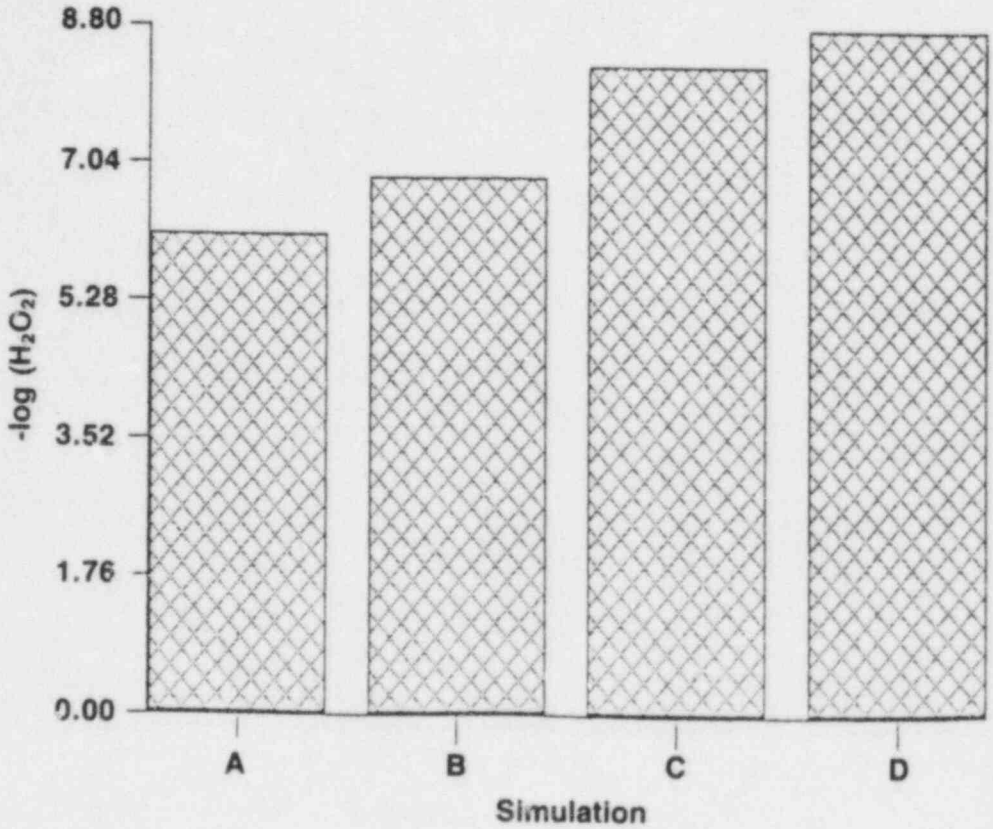

Figure 4.4. Concentration of H_2O_2 calculated at 3×10^4 seconds for each simulation.

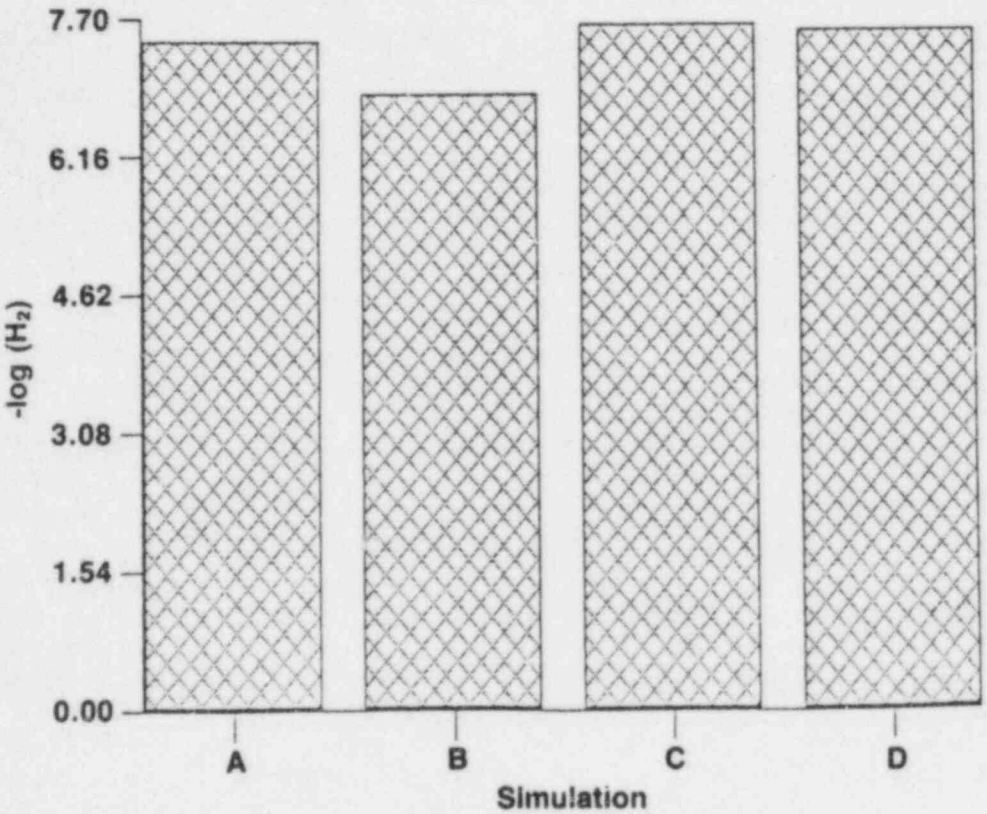

Figure 4.5. Concentration of dissolved hydrogen calculated at 3×10^4 seconds for each simulation.

be expected from experiments performed in unperturbed groundwater environments. Integral tests also provide a means of examining interactions between degraded waste-package components and waste-package performance; for example, interactions between radionuclide release rates and cladding degradation.

Spent-fuel integral experiments underway at Battelle combine characteristics of waste-package degradation and waste-package performance in a variety of environments containing packing material, simulated corrosion products, basalt chips, and simulated groundwaters. These experiments, by virtue of their principle components, are performed in a radiation field. The apparatus is assembled into two primary sections. One section, containing the spent-fuel materials and other types of samples, is located inside a hot cell. The in-cell component is housed in a oven which, for the current tests, is operated at a temperature of 90 C. The remainder of the apparatus is located outside the hot cell. Since the experiment uses a once-through flow design, the out-of-cell portion of the apparatus provides for both the source of simulated groundwater and the collection of aqueous effluents. A matrix of experiments which are underway and which are yet to be performed (in tuff environments) is shown in Table 4.4. Data shown in this report will reference the test numbers shown in this matrix.

4.3.1 Burnup Analyses

Part of the preoperational effort involved measuring the radionuclide inventory of representative spent-fuel samples. This inventory is to provide reasonable estimates of the initial radionuclide content of the spent-fuel waste forms used in the experiments. Part of this effort included burnup analyses of PWR and BWR spent-fuel materials by the ND-148 method[4.20]. For the purposes of the present calculations, the fission yield of ND-148 is assumed to be 1.671 percent. The materials were taken from sections of spent-fuel rods adjacent to the locations, in the same rod, from which sections were removed for use in the integral experiments. The analyses give the ratios of the various isotopes of uranium and plutonium, thus allowing radiochemical data to be transformed into chemical data for these elements. A precise determination of burnup also supports analytical calculations, via ORIGEN or ORIGEN II[4.21] computer codes, of the composition of the material. Results of the burnup analyses of the representative spent-fuel samples are shown in Tables 4.5 and 4.6. Table 4.5 shows the atom percent analysis for various uranium and plutonium isotopes and the $^{148}Nd/^{238}U$ and $^{239}Pu/^{238}U$ ratios. Table 4.6 shows the burnup values for the PWR and BWR fuel samples taken from the rods which were used to provide the spent-fuel samples for the integral experiments. Laboratory analyses of the elemental composition of spent-fuel samples is also underway to provide data on the pretest inventory of radionuclides in the spent-fuel specimens used in these experiments.

Table 4.4. Matrix of Integral Tests.

Test No.	Specimen	Fractional Area Exposed (%)	Flow Rate (ml/day)
1	PWR intact fuel-rod segment	0	1
2	PWR degraded fuel-rod segment (1/16 inch perforations)	.5	1
3	PWR degraded fuel-rod segment (1/16 inch perforations)	.5	1
4	PWR degraded fuel-rod segment (1/16 inch perforations)	3	1
5	PWR degraded fuel-rod segment (1/16 inch perforations)	3	1
6	PWR degraded fuel-rod segment (1/16 inch perforations)	15	1
7	PWR degraded fuel-rod segment (1/16 inch perforations)	15	1
8	PWR spent-fuel fragments	100	1
9	PWR spent-fuel fragments	100	1
10	PWR spent-fuel fragments	100	10
11	PWR spent-fuel fragments	100	10
12	BWR spent-fuel fragments	100	1
13	BWR spent-fuel fragments	100	1
14	PWR degraded fuel-rod segment (1/32-inch perforations)	3	1
15	PWR degraded fuel-rod segment (1/32-inch perforations)	3	1
16	BWR fuel-rod section with in-service failure	-	1
17	Test cancelled--fuel fell out of sample	-	1
18	BWR fuel-rod section with in-service failure	-	1

Table 4.4. Continued

Test No.	Specimen	Fractional Area Exposed (%)	Flow Rate (ml/day)
19	BWR fuel-rod section with in-service failure	-	1
20	PWR sections embedded in packing (1/16-inch perforation in each of 4 spent fuel-rod sections)	-	1
21	PWR cladding slit and with PWR cladding perforation embedded in packing (1/16-inch perforation and a 1/16-inch by 0.5-inch slit)	-	1
22	PWR cladding slit and with PWR cladding perforation embedded in packing (1/16-inch perforation and a 1/16-inch by 0.5-inch slit)	-	1
23	PWR fuel with cladding perforation embedded in corrosion products	-	1
24	PWR fuel with cladding slit embedded in corrosion products	-	1
25	PWR fuel fragments	-	1
26	PWR fuel fragments	-	1
27	PWR fuel fragments	-	1
28	PWR fuel fragments	-	1
29	Blank (control)	-	1
30	(not used)	-	1

Table 4.5. Results of heavy element analysis.

Sample and Axial Location*	Atom Percent U-234	U-235	U-236	U-238	Nd-148 / U-238	Pu-239 / U-238
PWR Aprox. 59	0.015	0.600	0.346	99.039	5.648×10^{-4}	5.022×10^{-3}
BWR Aprox. 89	0.019	1.394	0.243	98.344	2.826×10^{-4}	3.981×10^{-3}

	Plutonium Isotopes - Atom Percent Pu-238	Pu-239	Pu-240	Pu-241	Pu-242	Date of Analysis
PWR Aprox. 59	1.617	56.393	26.437	9.488	6.065	10-23-85
BWR Aprox. 89	0.540	72.041	19.908	6.103	1.408	10-23-85

* Inches from bottom of the rod.

Table 4.6. Calculated burnup values for PWR and BWR spent-fuel samples.

Sample Axial Location*	F' (Fission/Atoms U-238)	U' (Atoms U/Atoms U-238)	Pu' (Atoms Pu/Atoms U-238)	F_T (Atom % Burnup)	Burnup (MWD/MTU)**
PWR Aprox. 59	3.380×10^{-2}	1.0097	8.905×10^{-3}	3.212	30,835
BWR Aprox. 89	1.691×10^{-2}	1.0168	5.526×10^{-3}	1.627	15,619

* Inches from bottom of the rod.
** Megawatt days per metric ton uranium.

$$F' = \frac{\text{Nd-148}}{\text{U-238}} \times \frac{100}{1.671}$$

$$Pu' = \frac{\text{Pu-239}}{\text{U-238}} \times \frac{100}{\% \text{ Pu-239}}$$

$$F_T = \frac{F' \times 100}{U' + Pu' + F'}$$

$$\text{Burnup} = F_T \times 9.6 \times 10^3.$$

4.3.2 Data from the Spent-Fuel Integral Tests

The spent-fuel integral tests became operational on September 30, 1985. Of the 29 individual tests outlined in the test matrix shown in Table 4.4, all are operational except test no. 17 because the fuel fell out of the sample during preparation, and test nos. 25 to 28 because the tuff material has not been received yet. Since the samples were loaded in the hot cell in an air environment, the early data are not expected to be representative of the environment intended for the tests. As such, effluent from the first two months has been collected and stored for possible future analysis. Routine analyses of the effluent was initiated in December, 1985. Gamma analyses for two consecutive weeks of sampling during this period are described in this report. These data are shown in Figures 4.6 to 4.8. The data show the ^{134}Cs activity in uCi per ml for the effluent collected from the sample chambers containing the tests indicated for samples collected on 12/13/85 and 12/20/85. Since these data are from an early period of operation, some confounding influences are evident which will be corrected during the next quarter. In particular, there has been some difficulty with the temperature controller on the oven. Temperatures of 100 C and above were never observed, however. Also, the diameter of the sample exit lines (1/4 inch) is large enough for the effluent fluid to occasionally flow out of the lines. At flow rates of 1 and 10 ml/day, this can introduce significant error. This will be corrected by replacing the end sections of these lines with capillary tubing. As a result, some samples taken on 12/20/85 did not have enough fluid for a quantitative analysis. Data for these samples therefore are not reported, nor is data reported for samples where the specific activity level was below detectable limits.

Figure 4.6 shows the data for test nos. 1 to 7. These tests examine influences of cladding degradation on the release rates of radionuclides. Test no. 1 represents an intact capped fuel-rod segment. Since this sample showed the highest activity of this set, and since the unit activity is dropping rapidly, we believe that these early data are skewed by surface contamination of fine particulates which were picked up by the samples during the sectioning of the rods and final preparation of the sample specimens. Anticipating this difficulty, each fuel-rod segment was superficially cleaned with a damp cloth before insertion into its test chamber. With time, the specific activities for this set should become representative of the samples themselves.

Figure 4.7 shows the specific activities of the fluid collected from the test chambers for test nos. 8 to 13. These contain PWR and BWR fuel fragments. Since the specific activities are lower than for test nos. 1 to 7, we believe that the easily dissolved material was released at an early stage compared with the degraded fuel-rod specimens. To test this assumption, we will analyze the samples from the first two months of operation to determine the early activity releases.

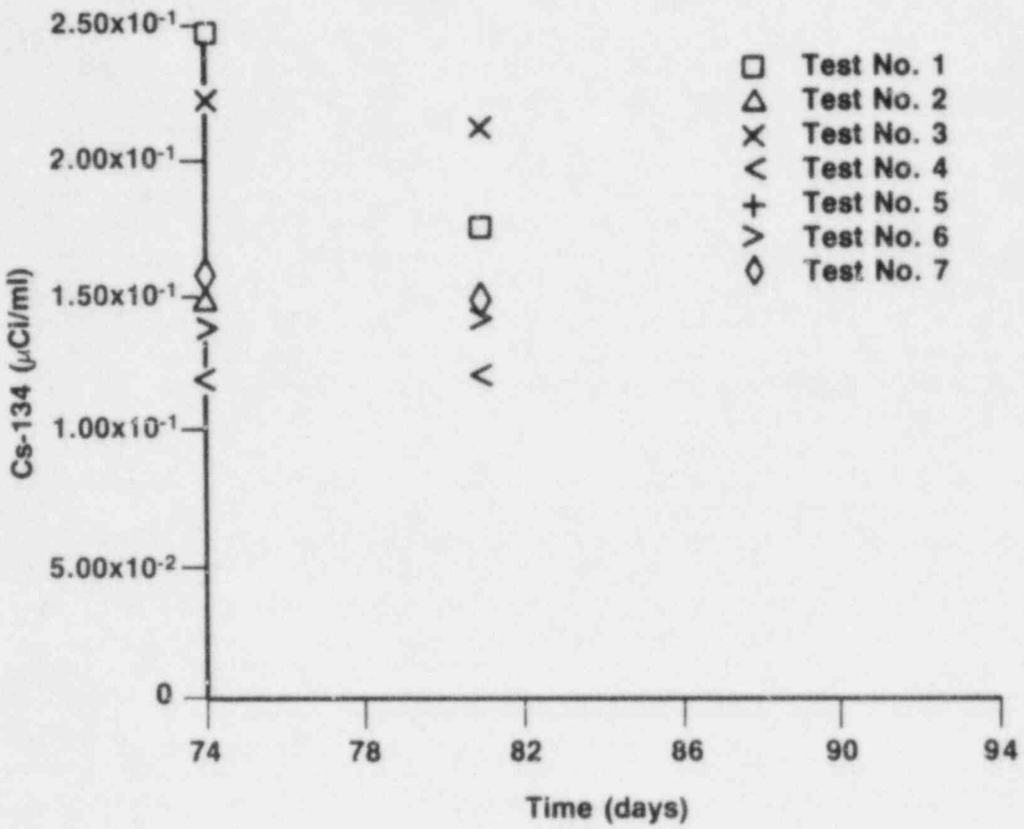

Figure 4.6. Specific activities of ^{134}Cs for the effluent collected for test nos. 1 to 7.

Data for test no. 5 is unavailable.

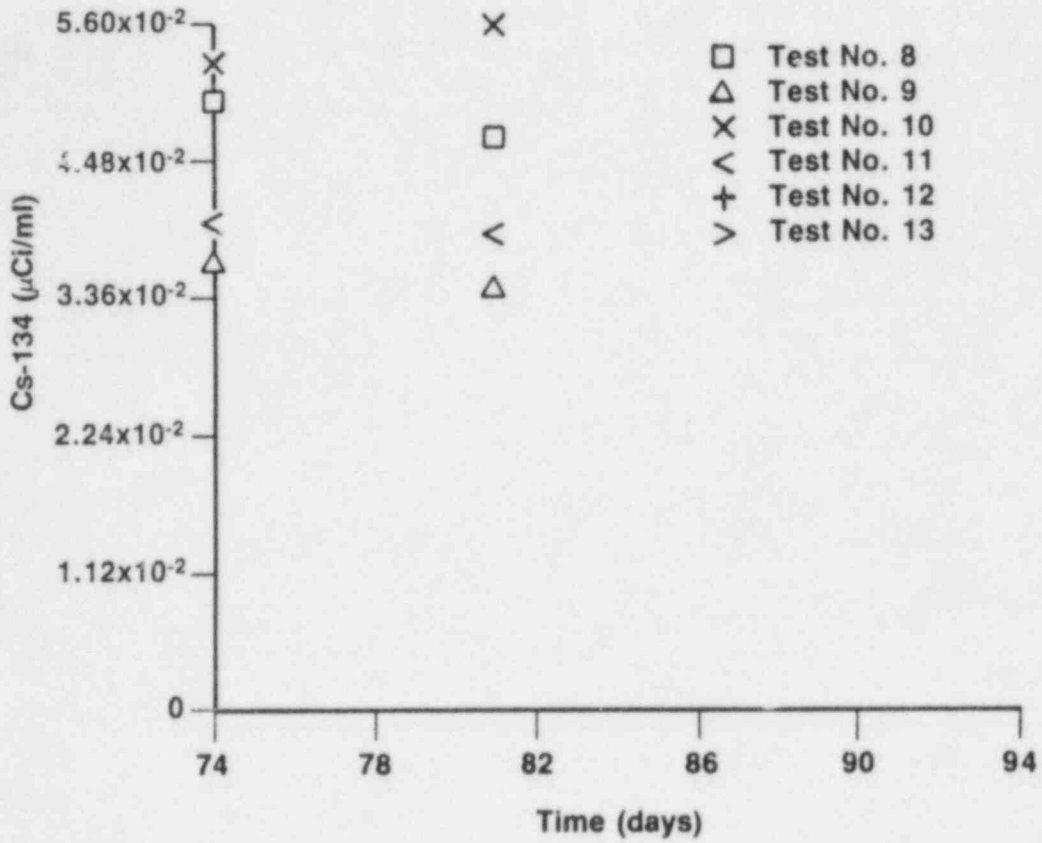

Figure 4.7. Specific activities of ^{134}Cs in the effluents for test nos. 8 to 13.

Data for test nos. 12 through 15 are unavailable.

Figure 4.8 shows the specific activity of ^{134}Cs in the effluent from sample chambers containing test nos. 16 to 19. These are for sample BWR spent-fuel rods containing possible in-service failures. The presence of these failures was estimated based on results of eddy current tests reported previously[4.22]. Activity releases were observed for test nos. 16 and 18.

4.3.3 Near-Term Plans

In the near term we will add hydrolysis of bicarbonate to the groundwater-radiolysis model. This will hopefully improve the calculation of pH when this species is present by providing additional hydroxide anions. Further extension of the model will continue, and the influences of chloride and related species on the oxidation of ferrous ions will be examined. Work in water-chemistry modeling will continue with further extension of the WATEQ module to account for the presence of spent-fuel species. Data collection from the integral experiments will continue. Also, samples of the early effluent will be analyzed to examine the early releases from the fuel fragments and degraded spent-fuel specimens. To remove known confounding influences, the temperature control of the oven will be improved, and the end sections of the exit lines will be replaced with capillary tubing.

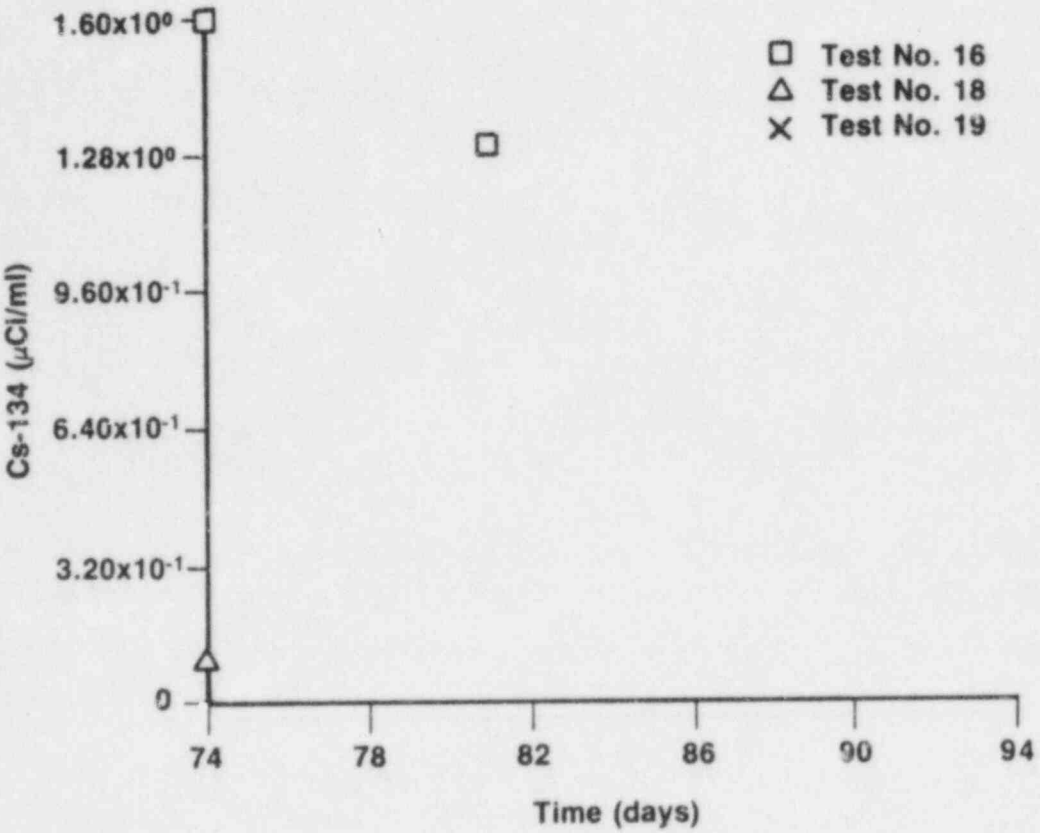

Figure 4.8. Specific activities of ^{134}Cs in the effluent for test nos. 16 to 19.

Data for test no. 19 is unavailable.

4.4 References for Section 4

(4.1) "Long-Term Performance of Materials Used for High-Level Waste Packaging", D. Stahl and N. E. Miller (Compilers), NUREG/CR-3900, Vol. 4, Annual Report (July 1985).

(4.2) T. D. Chikalla and J. A. Powell, "Nuclear Waste Management Semi-Annual Progress Report", (October 1982-March 1983), PNL-4250-3 (1983).

(4.3) Takashi Furuya, et al., "Study on Gamma-Ray Irradiation Effects on Corrosion Resistance of Alloys for Storage of High-Level Waste Packages", JAERI-M 82-061 (1982).

(4.4) "Long-Term Performance of Materials Used for High-Level Waste Packaging", D. Stahl and N. E. Miller (Compilers), NUREG/CR-3427, Vol. 4, Annual Report (June 1984).

(4.5) E. L. J. Rosinger and R. S. Dixon, "Mathematical Modeling of Water Radiolysis: A Discussion of Various Methods", AECL-5958 (1977).

(4.6) "Conceptual Waste Package Designs for Disposal of Nuclear Waste in Tuff", Westinghouse Electric Corporation, ONWI-439, p.73, (April 1983).

(4.7) "Engineered Waste Package System Design Specification", Westinghouse Electric Corporation, ONWI-423, p.28, (May 1983).

(4.8) S. G. Pitman and E. E. Hall, "Environmentally Assisted Fracture of Cast and Wrought Mild Steels in Brine", Waste Management 84, pp. 613-7 (1984).

(4.9) F. A. Cotton and G. Wilkinson, Advanced Inorganic Chemistry, second edition, p. 309, Interscience Publishers, New York, 1966.

(4.10) M. Eigen et al., "Rate Constants of Protolytic Reactions in Aqueous Solution", in Progress in Reaction Kinetics, Vol. 2, Porter, ed., (Pergamon, Oxford, 1964).

(4.11) J. L. Weeks and J. Rabani, "The Pulse Radiolysis of Deaerated Aqueous Carbonate Solutions. I. Transient Optical Spectrum and Mechanism. II. pK for OH Radicals", J. Phys. Chem. 70, 2100-6 (July 1966).

(4.12) Chemical Kinetics, Vol. 6, Reactions of Non-Metallic Inorganic Compounds, C. F. H. Tipper, ed., (Elsevier Publishing Company, New York, 1972) pp. 283-4.

(4.13) Keene et al., "Pulse Radiolysis Studies of Carboxyl and Related Radicals", Pulse Radiolysis, pp. 99-106.

(4.14) G. V. Buxton et al., "The Radiation Chemistry of Aqueous Solutions of Sodium Nitroprusside", Intl. J. Radiat. Phys. Chem. 1, 87-98 (1969).

(4.15) S. Nehari and J. Rabani, "The Reaction of H Atoms with OH^- in the Radiation Chemistry of Aqueous Solutions", J. Phys. Chem. 67, pp. 1609-13 (1963).

(4.16) K. B. Schmidt, "Electrical Conductivity Techniques fot Studying the Kinetics of Radiation-Induced Chemical Reactions in Aqueous Solutions", Intl. J. Radiat. Phys. Chem. 4, 439-68 (1972).

(4.17) R. R. Hentz et al., "Gamma Radiolysis of Liquids at High Pressures. III. Aqueous Solutions of Sodium Bicarbonate" J. Chem. Phys. 47, pp. 374-7 (1967).

(4.18) A. Barkatt et al., "Correlation Between Dynamic Leach Test Results and Geochemical Observations", Materials Research Society: Scientific Basis for Nuclear Waste Management VI", D. G. Brooks, ed., pp. 227-34 (1983).

(4.19) S. L. Nicolosi, "A Generalized Groundwater Radiolysis Model", Waste Management 85, 221-24 (1985).

(4.20) "Test Method for Atom Percent Fission in Uranium and Plutonium Fuel (Neodymium-148 Method)", ASTM E321-79 (1979).

(4.21) Croff, A. G., "ORIGEN 2--A Revised and Updated Version of the Oak Ridge Isotope Generation and Depletion Code", ORNL-5621 (July 1980).

(4.22) "Long-Term Performance of Materials Used for High-Level Waste Packaging", D. Stahl and N. E. Miller (Compilers), NUREG/CR-4379, Vol. 1, (June 1985), pp. 4-15 ff.

5. QUALITY ASSURANCE

Quality assurance standards have been established to monitor the various laboratory procedures and program activities. Procedures are revised and new ones prepared as necessary to meet program requirements. Four new procedures were either prepared or approved during this quarter, leaving a total of 38 approved QA procedures and 2 approved work instructions for the program.

A summary of the QA procedures which are being used in this program is given in Table 5.1. Included is the procedure number, the current revision number, the title, and the status.

Table 5.1. Status of NRC waste packaging program QA procedures.

Procedure No.	Title	Status
WF-PP-1 Revision 0	Procedures for Record Keeping and Documentation for NRC Waste Form System Model Development	Approved
WF-PP-5 Revision 0	Procedures for Record Keeping and Documentation for Separate Effects Model Development	Approved
WF-PP-10 Revision 0	Laboratory Procedure for Preparation of Glasses for NRC Waste Form Project	Approved
WF-PP-11 Revision 1	Laboratory Procedures for Preparation of Teflon-Leach Containers	Approved
WF-PP-14 Revision 1	Laboratory Procedure for Leaching Glass Samples	Approved
WF-PP-16 Revision 0	Laboratory Procedure for Operating the Orton Dilatometer	Approved
WF-PP-17 Revision 0	Laboratory Procedures for the Fluorometric Analysis of Uranium in Ground Water and Brine	Approved
WF-PP-18 Revision 0	Experimental Procedure for Flow-Through Leaching of Unirradiated UO_2 and Spent Fuel	To Be Written
WF-PP-20 Revision 0	Procedure for Determining the Corrosion Rates of Alloys at High Temperatures	Approved
WF-PP-25 Revision 0	Procedure for Preparation of Carbon-Steel Casting	Approved

Table 5.1. Continued.

Procedure No.	Title	Status
WF-PP-26 Revision 0	Procedure for Preparation of Steel Hydrogen-Embrittlement Test Specimens	Approved
WF-PP-26.1 Revision 0	Procedure for Preparation of Hydrogen-Embrittlement Test Specimens from Steel or Iron Samples	Approved
WF-PP-27 Revision 4	Procedure for J-Testing Compact Tension Specimens	Approved
WF-PP-27.1 Revision 0	Procedures for Performing Subcritical-Crack-Growth Tests with Compact Tension Specimens	Approved
WF-PP-28 Revision 1	Procedure for Performing Tension Tests of Steel Specimens	Approved
WF-PP-29 Revision 0	Procedure for Conducting Hydrogen-Absorption Experiments	Approved
WF-PP-30 Revision 0	Laboratory Procedure for Preparation, Cleaning, and Evaluation of Titanium Grade-12 Specimens for Corrosion Studies of the Overpack Performance for the NRC Waste Packaging Program	Approved
WF-PP-31 Revision 0	Laboratory Procedure for Preparation, Cleaning, and Evaluation of Cast and Wrought Carbon Steel Specimens for Corrosion Studies of the Overpack Performance for the NRC Waste Packaging Program	Approved
WF-PP-32 Revision 1	Laboratory Procedure for Preparation of Simulated WIPP Brine A	Approved

Table 5.1. Continued.

Procedure No.	Title	Status
WF-PP-33 Revision 0	Procedure for Preparation of Simulated Basalt Groundwater Solution	Approved
WF-PP-33.1 Revision 0	Procedure for Preparation of Basalt Rock for Use in Corrosion Studies for the NRC Waste Packaging Program	Approved
WF-PP-34 Revision 0	Laboratory Procedure for Preparation of Simulated Tuff Groundwater Solutions	Approved
WF-PP-35 Revision 1	Procedure for Performing Autoclave Exposures for Corrosion Tests in Simulated Brines	Approved
WF-PP-35.1 Revision 0	Procedure for Performing Autoclave Exposures for Corrosion Tests in Simulated Brines Using Sealed Internal Canister	Approved
WF-PP-36 Revision 0	Procedure for Performing Stagnant Autoclave Exposures for Corrosion Tests in Simulated Basalt or Tuff Groundwaters	Approved
WF-PP-37 Revision 0	Laboratory Procedure for Preparing Polarization Resistance Specimens, Performing Polarization Resistance Measurements and Evaluating Polarization Resistance Data	Approved
WF-PP-37.1 Revision 0	Laboratory Procedure for Performing Eh and Corrosion Potential Measurements in Autoclave Exposures in Simulated Basalt and Tuff Groundwater	Approved
WF-PP-37.2 Revision 0	Laboratory Procedure for Determination of the Polarization Behavior of Metal Specimens at Ambient Pressure	Approved
WF-PP-38 Revision 0	Procedure for Preparing and Evaluation of U-Bend Specimens for Stress Corrosion Studies of Overpack Materials for the NRC Waste Packaging Project	Approved

Table 5.1. Continued.

Procedure No.	Title	Status
WF-PP-38.1 Revision 0	Procedure for Performing and Evaluating 3 Point Bend Beam Specimens for Stress Corrosion Studies of Overpack Materials for NRC Waste Package Program	Approved
WF-PP-39 Revision 0	Procedure for Preparing, Testing and Evaluating Crevice Corrosion Specimens of Titanium Grade-12 and Cast Steel	Approved
WF-PP-40 Revision 0	Laboratory Procedures for Preparation, Cleaning, and Evaluation of Thermogalvanic and Heat-Transfer Specimens	Approved
WF-PP-41 Revision 0	Laboratory Procedures for Determination of Corrosion Rates Under Heat-Transfer Conditions	Approved
WF-PP-42 Revision 0	Laboratory Procedure for Determination of Thermogalvanic Corrosion Rates	Approved
WF-PP-43 Revision 0	Procedure for Welding Titanium Grade-12 Plate for Use in Corrosion Studies of Overpack Materials for NRC Waste Isolation Project	Approved
WF-PP-45 Revision 0	Laboratory Procedure for Preparing and Evaluating Slow Strain-Rate Specimens and for Performing Slow Strain-Rate Tests	Approved
WF-PP-45.1 Revision 0	Laboratory Procedures for Performing Slow Strain-Rate Tests Under Potentiostated Conditions	Approved
WF-PP-46 Revision 0	Procedure for Preparation of Titanium Grade-12 Corrosion Specimens with Metallic Iron Embedded in the Surface	Approved
WF-PP-47 Revision 0	Procedure for Preparing Specimens and Performing Electrochemical Pit Propogation Experiments on Carbon Steel	Approved

Table 5.1. Continued.

Procedure No.	Title	Status
WF-PP-50 Revision 0	Procedure for Inspection of Equipment for In-Cell Integral Experiments	In Review
WF-PP-51 Revision 0	Procedure for Collection of Samples for In-Cell Integral Experiments	In Review

DISTRIBUTION LIST

Office of Regulatory Research
Division of Radiation Programs and Earth Sciences
Mail Stop 1130 SS
U.S. Nuclear Regulatory Commission, Washington, D.C. 20555

Attn: Division Director/Deputy Director
E. F. Conti, Chief, Waste Management Branch
F. A. Costanzi
J. R. Randall
M. B. McNeil
K. S. Kim, Project Manager (15)

Division of Waste Management, NMSS
Mail Stop 623 SS
U.S. Nuclear Regulatory Commission, Washington, D.C. 20555

Attn: Division Director/Deputy Director
Chief, Engineering Branch
E. A. Wick
M. Tokar
K. C. Chang
Document Control Center

Division of Waste Management, NMSS
U.S. Nuclear Regulatory Commission
1955 Jadwin Ave - Suite 310A
Richland, WA 99352

Attn: R. Cook, BWIP Site Rep.

Advisory Committee on Reactor Safeguards
Mail Stop H-1016
U.S. Nuclear Regulatory Commission, Washington, D.C. 20555

Attn: Waste Management Subcommittee
R. C. Tang

Battelle's Columbus Division
505 King Avenue
Columbus, Ohio 43201-2693

Attn: D. Stahl, Program Manager (50)

DISTRIBUTION LIST (Continued)

Martin A. Molecke
Sandia National Lab
Albuquerque, NM 87185

Neville Pugh
National Bureau of Standards
Washington, D.C. 20234

Nicholas Grant
Department of Metallurgy
Massachusetts Institute
of Technology
Cambridge, MA 02139

Jerome Kruger
Corrosion Section
National Bureau of Standards
Washington, D.C. 20234

Don J. Bradley
Waste Package Programs
Battelle Pacific Northwest Labs
Richland, WA 99352

Allen G. Croff
Oak Ridge National Laboratory
P.O. Box X
Oak Ridge, TN 37830

Lynn Hobbs
Department of Materials Science
Massachusetts Institute of
Technology
77 Massachusetts Avenue
Cambridge, MA 02139

Richard E. Westerman
Pacific Northwest Lab.
P.O. Box 999
Richland, WA 99352

Edward J. Hennelly
Savannah River Lab.
Aiken, SC 29808

Arthur A. Bauer
Office of Crystalline Rock
Development
Battelle Memorial Institute
505 King Avenue
Columbus, OH 43201-2693

Michael Smith
Basalt Waste Isolation Projects
Rockwell Hanford Operation
Richland, WA 99352

Kenneth Russell
Department of Materials Science
and Engineering
Massachusetts Institute of
Technology
Cambridge, MA 02139

Robert H. Doremus
Materials Engineering Department
Rensselaer Polytechnic Institute
Troy, NY 12181

David C. Kocher
Oak Ridge National Lab.
P.O. Box X
Oak Ridge, TN 37830

Neville Moody
Sandia Livermore Lab.
Livermore, CA 94550

Donald E. Clark
ONWI
Battelle Memorial Institute
505 King Avenue
Columbus, OH 43201

Martin J. Steindler
Argonne National Lab.
Argonne, IL 60439

Donald G. Schweitzer
Brookhaven National Lab.
Upton, NY 11973

Peter Soo
Brookhaven National Lab.
Upton, NY 11973

Nestor Ortiz
Sandia National Lab.
Albuquerque, NM 87185

Pedro B. Macedo
Catholic University of America
Washington, D.C. 20064

DISTRIBUTION LIST (Continued)

Robert Williams
Electric Power Research Institute
P.O. Box 10412
Palo Alto, CA 94301

William P. Reed
U.S. Department of Commerce
National Bureau of Standards
Washington, D.C. 20234

Ray Walton
U.S. Department of Energy
Washington, D.C. 20545

John E. Mendel
Materials Characterization Center
Pacific Northwest Lab.
P.O. Box 999
Richland, WA 99352

Larry Hench
University of Florida
Gainesville, FL 32611

David E. Clark
University of Florida
Gainesville, FL 32611

Joseph Muscara
Mail Stop 1130 SS (5650 NL)
U.S. NRC
Washington, DC 20555

Ken W. Stephens
The Aerospace Corp., Suite 400
955 L'Enfant Plaza, S.W.
Washington, DC 20024

Robert S. Dyer
Office of Radiation Programs
(ANR-461)
U.S. Environmental Protection Agency
401 M Street, S.W.
Washington, DC 20460

Lorenzo Ricks
U.S. DOE/BES
Washington, D.C. 20545

Larry Evans
Armco Research Center
703 Curtis St.
Middletown, OH 45043

Robert R. Gaugh
Armco Research Center
703 Curtis St.
Middletown, OH 45043

M. John Plodinec
Savannah River Laboratory
Aiken, SC 29808

Robert H. Frost
Colorado School of Mines
Center for Welding Research
Golden, CO 80401

G.B. Birchard
Mail Stop 1130 SS
U.S. NRC
Washington, D.C. 20555

T.C. Johnson
Mail Stop 623 SS
U.S. NRC
Washington, D.C. 20555

John Voglewede
Mail Stop 623 SS
U.S. NRC
Washington, D.C. 20555

Document Control Center, NMSS
Mail Stop 623 SS
U.S. NRC
Washington, D.C. 20555

R.E. Browning/M.J. Bell
Mail Stop 623 SS
U.S. NRC
Washington, D.C. 20555

P.T. Prestholt
U.S. NRC
1050 Flamingo Rd. Suite 319
Las Vegas, NV 89119

DISTRIBUTION LIST (Continued)

W. Ott
Mail Stop 1130 SS
U.S. NRC
Washington, D.C. 20555

J.T. Greeves
Mail Stop 623 SS
U.S. NRC
Washington, D.C. 20555

T.L. Jungling
Mail Stop 623 SS
U.S. NRC
Washington, D.C. 20555

Tilak Verma
U.S. NRC - SRPO/ONWI
505 King Ave.
Columbus, OH 43201

Metal Component Subcommittee
Mail Stop H-1016, ACRS
U.S. NRC
Washington, D.C. 20555

Jack L. McElroy
Pacific Northwest Lab
P.O. Box 999
Richland, WA 99352

Harold Wallenberg
Lawrence Berkeley Lab
Berkeley, CA 94720

Don Alexander
U.S. DOE
Washington, D.C. 20545

NRC FORM 335 (2-84) NRCM 1102, 3201, 3202

U.S. NUCLEAR REGULATORY COMMISSION

BIBLIOGRAPHIC DATA SHEET

SEE INSTRUCTIONS ON THE REVERSE

1. REPORT NUMBER (Assigned by TIDC, add Vol. No., if any)

NUREG/CR-4379, Vol. 3

2. TITLE AND SUBTITLE

Long-Term Performance of Materials Used for High-Level Waste Packaging, Third Quarterly Report, Year Four October - December 1985

3. LEAVE BLANK

4. DATE REPORT COMPLETED

MONTH: February YEAR: 1986

5. AUTHOR(S)

Compiled by D. Stahl and N.E. Miller

6. DATE REPORT ISSUED

MONTH: March YEAR: 1986

7. PERFORMING ORGANIZATION NAME AND MAILING ADDRESS (Include Zip Code)

Battelle's Columbus Division
505 King Avenue
Columbus, Ohio 43201-2693

8. PROJECT/TASK/WORK UNIT NUMBER

9. FIN OR GRANT NUMBER

B6764

10. SPONSORING ORGANIZATION NAME AND MAILING ADDRESS (Include Zip Code)

Division of Radiation Programs and Earth Sciences
Office of Nuclear Regulatory Research
U.S. Nuclear Regulatory Commission
Washington, D.C. 20555

11a. TYPE OF REPORT

Quarterly

b. PERIOD COVERED (Inclusive dates)

October - December 1985

12. SUPPLEMENTARY NOTES

13. ABSTRACT (200 words or less)

Waste-form studies are being directed toward investigating spent-fuel leaching/dissolution behavior. Experiments have been started to generate data on UO_2 and spent-fuel leach rates in simulated anoxic groundwaters. Initial data indicate that uranium concentrations in the groundwaters and distilled-water leachants are very low. The influence of groundwater species on the susceptibility of cast steel to pitting corrosion and stress-corrosion cracking is being studied by potentiodynamic polarization techniques. Potential cracking agents are being investigated by slow strain rate experiments. The pitting-corrosion model was further developed, taking into account cation dissolution at the pit base and chemically active pit walls. Groundwater-radiolysis modeling has continued, with the description being extended to include bicarbonate anions in groundwater. Simulations show that modifications to the reactions accounting for bicarbonate should improve predicted pH values. Spent-fuel specimens are being used in integral tests with flowing simulated groundwater to study the role of cladding in radionuclide release and to identify possible combined-effects processes.

14. DOCUMENT ANALYSIS - a. KEYWORDS/DESCRIPTORS

High-level waste
Waste package
Waste form/overpack

b. IDENTIFIERS/OPEN ENDED TERMS

15. AVAILABILITY STATEMENT

Unlimited

16. SECURITY CLASSIFICATION

(This page) Unclassified

(This report) Unclassified

17. NUMBER OF PAGES

18. PRICE

UNITED STATES
NUCLEAR REGULATORY COMMISSION
WASHINGTON, D.C. 20555

OFFICIAL BUSINESS
PENALTY FOR PRIVATE USE, $300

SPECIAL FOURTH CLASS RATE
POSTAGE & FEES PAID
USNRC
WASH D.C.
PERMIT No. G-67

120555078877 1 1AN1CH
US NRC
ADM-DIV OF TIDC
POLICY & PUB MGT BR-PDR NUREG
W-501
WASHINGTON DC 20555